Title: Severe COVID-19 Is Fueled by Disrupted Gut Barrier Integrity

Short title: COVID-19 and Gut Functionality

Authors: Leila B. Giron[1], Harsh Dweep[1], Xiangfan Yin[1], Han Wang[1], Mohammad Damra[1], Aaron R. Goldman[1], Nicole Gorman[1], Clovis S. Palmer[2,3], Hsin-Yao Tang[1], Maliha W. Shaikh[4], Christopher B. Forsyth[4], Robert A. Balk,[4] Netanel F Zilberstein,[4] Qin Liu[1], Andrew Kossenkov[1], Ali Keshavarzian[4], Alan Landay[4], Mohamed Abdel-Mohsen[1*]

Affiliations: [1]The Wistar Institute, Philadelphia, PA, 19104, USA; [2]The Burnet Institute, Melbourne, Victoria, 3004, Australia; [3]Department of Infectious Diseases, Monash University, Melbourne, Victoria, 3004, Australia; [4]Rush University, Chicago, IL, 60612, USA;

[*]Corresponding author: Mohamed Abdel-Mohsen, Ph.D. Assistant Professor, Vaccine and Immunotherapy Center, The Wistar Institute. 3601 Spruce Street, Philadelphia, PA 19104. Phone: 215-898-6008. Email: mmohsen@Wistar.org

ABSTRACT

A disruption of the crosstalk between gut microbiota and the lung (gut-lung axis) has been implicated as a driver of severity during respiratory-related diseases. Lung injury causes systemic inflammation, which disrupts gut barrier integrity, increasing the permeability to gut microbes and their products. This exacerbates inflammation, resulting in positive feedback. To test the possibility that a disrupted gut contributes to Coronavirus disease 2019 (COVID-19) severity, we used a systems biology approach to analyze plasma from COVID-19 patients with varying disease severity and controls. Severe COVID-19 is associated with a dramatic increase in tight junction permeability and translocation of bacterial and fungal products into blood. This intestinal disruption and microbial translocation correlate strongly with increased systemic inflammation and complement activation, lower gut metabolic function, and higher mortality. Our study highlights a previously unappreciated factor with significant clinical implications, disruption in gut barrier integrity, as a force that contributes to COVID-19 severity.

Key Words: SARS-CoV2; COVID-19; Gut; Microbial Translocation; Microbial Dysbiosis; Metabolic; Glycomic, Citrulline; Zonulin; Galectin.

INTRODUCTION

Coronavirus Disease 2019 (COVID-19), the disease caused by severe acute respiratory syndrome coronavirus 2 (SARS-CoV-2) infection, can manifest with diverse clinical presentations. While the majority of infected individuals exhibit asymptomatic or mild respiratory tract infection, a significant population, especially those who are older or suffering from pre-existing metabolic-associated diseases, face severe manifestations such as acute respiratory distress syndrome (ARDS), multi-organ failure, and death.[1-5] A state of hyper-inflammation and hyperactivated immune responses, characterized by an ensuing cytokine storm and increased complement activation, has been associated with COVID-19 severity.[1,6-10] However, the pathophysiological mechanisms that contribute to these phenomena remain mostly unknown. Understanding these mechanisms is a crucial step in designing rational clinical and therapeutic strategies.

A disruption of the crosstalk between gut microbiota and the lung (gut-lung axis) has been implicated as a driver of severity during respiratory-related diseases, including ARDS.[11-14] Systemic inflammation caused by a lung infection or injury can lead to a disruption of the gut barrier integrity and increase the permeability to gut microbes and microbial products. This microbial translocation can exacerbate systemic inflammation and lung injury – resulting in positive feedback.[11-14] In addition, SARS-CoV2 can directly infect gut cells,[15] and viral infections of the gut cause changes in gut structure[16] and breakdown of the epithelial barrier.[17,18] Such disruption of the gut-lung axis is more likely to occur in older individuals and individuals with metabolic- and/or aging-associated diseases, as these individuals often experience changes in the composition of the gut microbiota (microbial dysbiosis),[19,20] which facilitate a higher susceptibility to falling into the vicious cycle between microbial translocation and systemic inflammation.[21-24]

Even as microbial translocation impacts systemic inflammation directly, it may also impact it indirectly by modulating circulating levels of gut- and gut microbiota-associated products such as metabolites and lipids. Plasma metabolites and lipids can reflect the functional status of the gut and the metabolic activity of its microbiota.[25-28] They also are biologically active molecules in their own right, regulating several immunological functions, including inflammatory responses.[29,30] A third class of microbial products that can translocate from the gut is glycan-degrading enzymes. Glycans on circulating glycoproteins and antibodies (IgGs and IgAs) are

30 essential for regulating several immunological responses, including complement activation.[31] The
31 glycan-degrading enzymes are released by several members of the gut microbiome and their
32 translocation can alter the circulating glycome, leading to higher inflammation and complement
33 activation.[32] Indeed, altered glycosylation of plasma glycoproteins (including immunoglobulin G,
34 IgG) has been associated with the onset and progression of inflammatory bowel disease (IBD).[32-
35 37] Furthermore, modulation of the gut microbiota via fecal microbiota transplantation affects IgG
36 and serum glycosylation.[38] Here, we hypothesized that a vicious cycle between SARS-CoV2
37 infection, systemic inflammation, disrupted intestinal barrier integrity, and microbial translocation
38 contributes to COVID-19 severity.

39 To test this hypothesis, we applied a multi-omic systems biology approach to analyze plasma
40 samples from 60 COVID-19 patients with varying disease severity and 20 age-controlled (most
41 were 50 to 65 years old) and gender-matched (~50% female) SARS-CoV2 negative controls. We
42 investigated the potential links between gut barrier integrity, microbial translocation, systemic
43 inflammation, and COVID-19 severity. Our data indicate that severe COVID-19 is associated with
44 a dramatic increase in tight junction permeability and translocation of bacterial and fungal products
45 into the blood. This disrupted intestinal barrier integrity and microbial translocation correlates
46 strongly with increased systemic inflammation, increased immune activation, decreased intestinal
47 function, disrupted plasma metabolome and glycome, and higher mortality rate.

48 **RESULTS**

49 ***Characteristics of the study cohort and study overview.*** We collected plasma samples from 60
50 individuals testing positive for SARS-CoV2 (by RT-PCR) and 20 SARS-CoV2 negative controls.
51 The 60 SARS-CoV2 positive individuals were selected to represent three diseases states: 20 with
52 mild symptoms (outpatients); 20 with moderate symptoms (inpatients hospitalized on regular
53 wards); and 20 with severe symptoms (inpatients hospitalized in an intensive care unit (ICU))
54 (**Figure 1a**). Individuals were selected to have a median age between 52.5 to 58.5 years to avoid
55 age bias in disease outcome. The study cohort was also chosen to have a 35 to 60% representation
56 of female gender per disease status group (**Supplementary Table 1**). Samples from hospitalized
57 patients (moderate and severe groups) were collected at the time of diagnosis when the patient was
58 admitted (**Supplementary Table 1**). Eight individuals of the cohort (two from the moderate group
59 and six from the severe group) died from COVID-19 (**Supplementary Table 1**). The plasma
60 samples from all individuals were used in a multi-omic, systems biology approach that measured:
61 markers of tight junction permeability and microbial translocation using ELISA and Limulus
62 Amebocyte Lysate assays; inflammation and immune activation/dysfunction markers using
63 ELISA and multiplex cytokine arrays; untargeted metabolomic and lipidomic analyses using mass
64 spectrometry (MS); and plasma glycomes (from total plasma glycoproteins, isolated
65 immunoglobulin G (IgG), and isolated immunoglobulin A (IgA)) using capillary electrophoresis
66 and lectin microarray (**Figure 1a** and **Supplementary Table 2**).

67 ***Severe COVID-19 is associated with high tight junction permeability and microbial***
68 ***translocation.*** We first asked whether severe COVID-19 is associated with changes in tight
69 junction permeability and microbial translocation. We measured the plasma levels of eight
70 established drivers and markers of intestinal barrier integrity (**Supplementary Table 2**). We found
71 that severe COVID-19 is associated with a dramatic increase in zonulin levels (**Figure 1b**).
72 Zonulin (haptoglobin 2 precursor) is the only known physiological mediator of tight junction
73 permeability in the digestive tract, where higher levels of zonulin drive increases in tight junction
74 permeability.[39] Notably, hospitalized individuals with higher plasma levels of zonulin were more
75 likely to die compared to hospitalized individuals with lower levels of zonulin (**Figure 1c**).

76 These higher levels of zonulin should enable the translocation of microbes and their products from
77 the gut into the blood, including parts of the cell wall of bacteria and fungus.[40,41] To test this
78 supposition, we measured plasma levels of common bacterial and fungal markers. Exposure to
79 bacterial endotoxin can be determined by measuring plasma lipopolysaccharide (LPS) binding
80 protein (LBP). LBP is an acute-phase protein that binds to LPS to induce immune responses.[42]
81 Indeed, we observed a systematic induction of LBP in individuals with severe COVID-19
82 compared to individuals with mild COVID-19 or controls (**Figure 1d)**. We also found higher levels
83 of β-glucan, a polysaccharide cell wall component of most fungal species and a marker of fungal
84 translocation,[43] in individuals with severe COVID-19 compared to those with mild COVID-19 or
85 controls (**Figure 1e**). In addition, there was a significant induction (FDR=0.025) of the tight
86 junction protein occludin in the severe group compared to controls (data not shown). There also
87 was a strong trend (FDR = 0.051) toward higher levels of the protein 3-alpha (REG3α), a marker
88 of intestinal stress,[44] comparing the severe and mild groups (data not shown). We did not observe
89 an increase in intestinal fatty-acid binding protein (I-FABP), a marker of enterocyte apoptosis,
90 suggesting that the increased levels of tight junction permeability and microbial translocation are
91 not associated with enterocyte death.

92 These high levels of tight junction permeability and microbial (both bacterial and fungal)
93 translocation are expected to lead to microbial-mediated myeloid inflammation. Indeed, levels of
94 soluble CD14 (sCD14; monocyte inflammation marker) (**Figure 1f**) and myeloperoxidase (MPO;
95 neutrophil inflammation marker) (**Figure 1g**) were significantly increased during severe COVID-
96 19. Levels of soluble CD163 (sCD163) were also increased significantly (FDR=0.04) in the severe
97 group compared to controls (data not shown). These data indicate that COVID-19 severity and
98 associated mortality are linked to higher tight junction permeability and higher translocation of
99 bacterial and fungal products to the blood.

100 ***Microbial translocation is linked to systemic inflammation.*** Higher levels of microbial
101 translocation should lead to higher systemic inflammation and immune dysfunction. We measured
102 the levels of 31 markers of systemic inflammation and immune activation/dysfunction
103 (**Supplementary Table 2**) including: 23 cytokines and chemokines (such as IL-6, IL-1β, MCP-1,
104 IP-10, and TNFα), markers of inflammation and thrombogenesis (such as C-reactive protein (CRP)
105 and D-dimer), a marker of complement activation (C3a), a marker of oxidative stress (GDF-15),

106 and three immunomodulatory galectins (galectin-1, -3, and -9). As anticipated, many of these
107 markers were increased in patients with severe COVID-19 compared to patients with mild
108 COVID-19 or controls (**Figure 2a-left**). In particular, we observed inductions in several cytokines
109 (such as IL-6 and IL-1β) and inflammatory markers (such as CRP and d-dimer). In addition to the
110 expected changes, we also observed significant inductions in the immunomodulatory lectins
111 galectin-3 (**Figure 2b**) and galectin-9 (**Figure 2c**). Levels of Gal-9 were higher in the plasma of
112 hospitalized patients who eventually died compared to survivors (**Figure 2d**). Last, notable
113 dysregulations were observed in levels of C3a (**Figure 1e**; indicative of complement activation)
114 and GDF-15 (**Figure 1f**; indicative of oxidative stress), with the levels of GDF-15 higher in
115 deceased hospitalized patients compared to survivors (**Figure 1g**).

116 Next, we examined the correlations between the markers of intestinal barrier integrity (zonulin) or
117 microbial translocation (LBP and β-glucan) and the 31 markers of systemic inflammation and
118 immune activation. As shown in **Figure 2a-right**, higher levels of zonulin, LBP, or β-glucan were
119 strongly positively correlated with higher levels of many of the markers of systemic inflammation
120 and immune activation, including IL-6 (**Figure 2h-i**). These data support our hypothesis that
121 disruption of intestinal barrier integrity, which results in microbial translocation, is linked to higher
122 systemic inflammation and immune activation during severe COVID-19.

123 ***Severe COVID-19 is associated with a plasma metabolomic profile that reflects disrupted gut***
124 ***function.*** A second set of factors that reflect the functional state of the gut and its microbiota are
125 the plasma metabolites. Importantly, many of these are not solely biomarkers of gut
126 function/dysfunction, but also are biologically active molecules which can directly impact
127 immunological and inflammatory responses. We performed untargeted metabolomic analysis
128 (using LC-MS/MS) on the plasma samples of the same cohort. Within the 80 plasma samples, we
129 identified a total of polar 278 metabolites. We observed a significant metabolomic shift during
130 severe COVID-19 (**Figure 3a**, a list of the top 50 dysregulated metabolites is in **Supplementary**
131 **Figure 1**). Indeed, in principal component analysis of the full metabolomic dataset, the first
132 component was able to completely distinguish controls (and mild patients) from those with severe
133 disease. Pathway analysis of the COVID-19-dysregulated metabolites showed disruption in tRNA
134 charging, citrulline metabolism, and several other amino acid (AA) metabolic pathways (**Figure**
135 **3b,** the top 10 dysregulated metabolic pathways are shown; **Supplementary Table 3** shows the

136 top 50 dysregulated metabolic pathways with FDR<0.05). Importantly, changes in AA
137 metabolism, including citrulline, arginine, methionine, and tryptophan (see **Figure 3b**), are not
138 only markers for gut dysfunction but also can influence the AA-metabolizing bacterial
139 communities and disrupt the gut-microbiome immune axis.[45,46] AA are absorbed and metabolized
140 by enterocytes and gut microbiota. Consumption of AA by the gut microbiome is important for
141 bacterial growth and is involved in the production of key microbiome-related metabolites.[46] These
142 metabolites can influence epithelial physiology and be sensed by immune cells to modulate the
143 mucosal immune system.[47,48]

144 Next, we focused on 50 of the metabolites (out of the total of 278) that are known to be associated
145 with the function of the gut and its microbiota (**Supplementary Table 4** lists the 50 metabolites
146 and their references). Levels of most of these gut-associated plasma metabolites (35 out of 50)
147 were dysregulated during severe COVID-19 compared to mild disease or controls (**Table 1** and
148 **Figure 3c**). Within this metabolic signature of COVID-19-associated gut dysfunction is citrulline,
149 which is also identified as a top metabolic pathway dysregulated by severe COVID-19 (**Figure**
150 **3c**). Citrulline is an amino acid produced only by enterocytes and an established marker of gut and
151 enterocyte function.[25] Its levels are significantly decreased during severe COVID-19 (**Figure 3d)**.
152 Also, within this metabolic signature is succinic acid, a well-established marker of gut microbial
153 dysbiosis, whose levels are increasing during severe COVID-19 (**Figure 3e**).

154 Notable changes were also observed in several metabolites involved in the catabolism of the AA
155 tryptophan (**Figure 3b, c**). Higher levels of tryptophan catabolism, indicated by high levels of
156 kynurenine and low levels of tryptophan (i.e. the [Kyn/Trp] ratio), is an established marker of gut
157 microbial dysbiosis.[49,50] Indeed, we observed a higher [Kyn/Trp] ratio in individuals with severe
158 COVID-19 than in those with mild disease or controls (**Figure 3f**). Furthermore, lower levels of
159 tryptophan and higher levels of kynurenic acid were associated with mortality among hospitalized
160 COVID-19 patients (**Figure 3g-h**). Together, these data indicate that a metabolic signature
161 associated with severe COVID-19 is compatible with disrupted gut functions and dysregulated
162 gut-microbiome axis.

163 ***Plasma metabolomic markers of COVID-19-associated gut dysfunction associate with higher***
164 ***inflammation and immune dysfunction.*** As noted above, many plasma metabolites are bioactive

165 molecules that can directly impact immunological and inflammatory responses. Therefore, we
166 sought to identify links between the 35 dysregulated gut-associated plasma metabolites (**Table 1**)
167 and the dysregulated markers of microbial translocation, inflammation, and immune activation
168 (**Figure 2a**). We observed strong links between levels of the dysregulated gut-associated
169 metabolites and levels of markers of microbial translocation (**Figure 4a**) as well as levels of
170 inflammation and immune activation (**Figure 4b**). Notable correlations were observed between
171 lower levels of citrulline and higher IL-6 (**Figure 4c**), higher levels of succinic acid and higher IL-
172 6 (**Figure 4d**), and higher [Kyn/Trp] ratio and higher IL-6 (**Figure 4e**). These data highlight the
173 potential links between disrupted metabolic activities, especially those related to the gut and its
174 microbiota, and systemic inflammation and immune dysfunction during COVID-19.

175 ***Severe COVID-19 is associated with disrupted lipid metabolism.*** Intermediary metabolites and
176 sulfur-containing amino acids (e.g. methionine, a regulated COVID-19 pathway, **Figure 3b**) are
177 potent modulators of lipid metabolism. Therefore, we performed lipidomic analysis on the plasma
178 samples of the same cohort. We identified a total of 2015 lipids using untargeted MS. Similar to
179 the plasma metabolome, the plasma lipidome shifted significantly during severe COVID-19
180 (**Figure 5a)**. These 2015 lipids were divided into 24 lipids classes (**Supplementary Table 5**); out
181 of these 24 classes, 16 were significantly (FDR<0.05) modulated by severe COVID-19 (11 were
182 downregulated whereas five were upregulated) (**Figure 5b**). Pathway analysis of this severe-
183 COVID-19-associated lipidomic signature showed that glycerophospholipid and choline
184 metabolism were the most significantly dysregulated pathways (**Figure 5c**). The gut microbiota is
185 heavily involved in these two interconnected pathways.[51] Gut microbial dysbiosis can alter the
186 digestion and absorption of glycerophospholipids, leading to several diseases.[51-54] These data
187 provide yet another layer of evidence that severe COVID-19 is associated with systemic
188 dysregulations that are linked to disrupted gut function.

189 ***Severe COVID-19 is associated with altered plasma glycomes that are linked to inflammation***
190 ***and complement activation.*** Finally, we examined plasma glycomes. It has been reported that
191 translocation of glycan-degrading enzymes released by several members of the gut microbiome
192 can alter circulating glycomes.[32] Within the plasma glycome, glycans on circulating glycoproteins
193 and antibodies (IgGs and IgAs) play essential roles in regulating several immunological responses,
194 including complement activation.[31] For example, galactosylated glycans link Dectin-1 to Fcγ

195 receptor IIB (FcγRIIB) on the surface of myeloid cells to prevent inflammation mediated by
196 complement activation.[31] A loss of galactose decreases the opportunity to activate this anti-
197 inflammatory checkpoint, thus promoting inflammation and complement activation, including
198 during IBD.[32,34-37] Indeed, IgG glycomic alterations associate with IBD disease progression and
199 IBD patients have lower IgG galactosylation compared to healthy controls.[33]

200 We applied several glycomic technologies to analyze the plasma glycome (total plasma, isolated
201 IgG, and isolated IgA). First, we used capillary electrophoresis to identify the *N*-linked glycans of
202 total plasma glycoproteins and isolated plasma IgG (this identified 24 and 22 glycan structures,
203 respectively; their names and structures are in **Supplementary Tables 6 and 7**). We also used a
204 45-plex lectin microarray to identify other glycans on total plasma glycoproteins and isolated IgA.
205 The lectin microarray enables sensitive analysis of multiple glycan structures by employing a panel
206 of 45 immobilized lectins (glycan-binding proteins) with known glycan-binding specificity
207 (**Supplementary Table 8** lists the 45 lectins and their glycan-binding specificities).[55]

208 We first observed a significant (FDR<0.05) glycomic alteration during severe COVID-19 in levels
209 of IgA glycans, plasma *N*-glycans, plasma total glycans, and IgG glycans (**Figure 6a)**. These
210 changes are exemplified by an apparent loss of the anti-complement activation galactosylated
211 glycans from IgG and total plasma glycoproteins (**Figure 6b-c**, respectively). When we examined
212 the correlations between the plasma glycome and markers of tight junction permeability/microbial
213 translocation or inflammation/immune activation (**Supplementary Figure 2**), as expected, we
214 observed significant negative correlations (FDR<0.05) between levels of terminal galactose on
215 IgG or plasma glycoproteins and markers of permeability/ translocation (**Figure 6d**) or markers of
216 inflammation (**Figure 6e**). These data highlight the potential links between the disrupted plasma
217 glycome and systemic inflammation during COVID-19.

218 ***Multivariable logistic models, using cross-validation Lasso technique, selected gut-associated***
219 ***variables whose combination associates with the risk of hospitalization during COVID-19.*** Our
220 data thus far support the hypothesis that gut dysfunction fuels COVID-19 severity. We sought to
221 examine whether markers of tight junction permeability and microbial translocation
222 (**Supplementary Table 2**) can distinguish between hospitalized COVID-19 patients (moderate
223 and severe groups combined) and non-hospitalized individuals (mild and controls combined). We

224 applied the machine learning algorithm Lasso (least absolute shrinkage and selection operator)
225 regularization to select markers with the highest ability to distinguish between the two groups. The
226 analysis employed samples with complete data sets (n=79; one sample did not have complete data).
227 Lasso selected zonulin, LBP, and sCD14 as the three markers to be included in a multivariable
228 logistic regression model that distinguishes hospitalized from non-hospitalized individuals with
229 area under the ROC curve (AUC) of 99.23% (**Figure 7a**; 95% confidence interval: 98.1% -100%).
230 This value was higher than the AUC values obtained from logistic models using each variable
231 individually (**Table 2).**

232 Next, we used the multivariable logistic model to estimate a risk score of hospitalization for each
233 individual. We then examined the ability of these risk scores to classify hospitalized from non-
234 hospitalized individuals. As shown in **Figure 7b**, the model correctly classified 97.5% of
235 hospitalized (sensitivity) and 94.9% of non-hospitalized (specificity) individuals, with an overall
236 accuracy of 96.2%. Furthermore, we examined the ability of the L-kynurenine/L-tryptophan
237 [Kyn/Trp] ratio, an established marker of gut microbial dysbiosis described above, to distinguish
238 hospitalized from non-hospitalized individuals. Logistic model showed that [Kyn/Trp] ratio alone
239 can distinguish hospitalized from non-hospitalized with an AUC value of 91.9% (**Figure 7c**; 95%
240 confidence interval: >85% -98.7%). This analysis further highlights the plausible link between
241 severe COVID-19 and disrupted gut function, orchestrated by an increase in tight junction
242 permeability, microbial translocation, possible microbial dysbiosis, and dysregulated digestion and
243 metabolism.

244 **DISCUSSION**

245 We used a systems biology approach to provide multiple layers of evidence that severe COVID-
246 19 is associated with a disruption in intestinal barrier integrity, higher microbial translocation, and
247 intestinal dysfunction. These data highlight a previously unappreciated factor, disruption in gut
248 barrier integrity, as a force that likely fuels COVID-19 severity. Our results do not imply that
249 microbial dysbiosis and translocation are the primary triggers of severe COVID-19, as the complex
250 clinical syndrome of severe COVID-19 likely embodies multiple pathophysiological pathways.
251 Also, our *in vivo* analyses do not unequivocally demonstrate a causal relationship between gut
252 dysfunction and COVID-19 severity. However, the robust literature indicating that a disrupted
253 intestinal barrier and microbial dysbiosis and translocation fuel inflammation and disease severity
254 during ARDS[11-14] supports our hypothesis and is consistent with our findings.

255 SARS-CoV-2 infection can affect the gastrointestinal tract (GI) tract and cause GI symptoms.[56,57]
256 Recently, it has been suggested that the severity of GI symptoms (mainly vomiting and diarrhea)
257 correlates inversely with COVID-19 severity (for unclear reasons).[58] On the other hand, our
258 observations suggest that disruption in gut function and higher microbial translocation correlate
259 positively with COVID-19 severity. These are not necessarily mutually exclusive findings, but
260 rather indicate that the interplay between the gut and SARS-CoV2 infection in modulating disease
261 severity is complex. The potential role of the gut should be further explored, in multiple cohorts
262 and settings, longitudinally during different stages of infection, and using gut biopsies and stool
263 samples.

264 Our data raise several critical questions, including are there long-term implications of a disrupted
265 gut barrier and intestinal function in survivors of severe COVID-19? In survivors of SARS-CoV-
266 1 infection, long-term health complications (including metabolic dysfunctions) were observed for
267 many years after convalescence.[59,60] HIV+ individuals also can suffer complications of gut
268 microbial translocation for years after viral suppression.[61-63] The current 'long-haulers' after severe
269 COVID-19 may also be on a path towards long term consequences due to persistent, microbial
270 translocation. Thus, understanding the long-term implications of the disrupted gut function that we
271 observed during severe COVID-19 should be a clinical priority. An accompanying priority should
272 be to consider how to modify clinical practice to prevent or reduce gut disruption. Currently, for

273 example, a large number of patients are receiving antibiotic therapy during their COVID-19
274 treatment.[1,5] However, massive use of antibiotics can alter gut microbiota and gut function, leading
275 to higher susceptibility to inflammatory disorders.[64] Thus, for any clinical practices that alter the
276 gut, their overall impact on disease course should be carefully considered, especially for older
277 patients and those with metabolic diseases, who are likely to have a lower threshold for intestinal
278 dysfunction.

279 Our study raises the possibility that some of the markers we identified through our multi-omic
280 approach may be able to predict the risk of disease progression if measured immediately after
281 diagnosis. The plasma is a pool of biological molecules, including polar metabolites, lipids, and
282 glycoproteins, secreted or shed from multiple tissues. Thus, the levels of these molecules likely
283 indicate the overall status of multiple organs, making them excellent candidates for biomarker
284 discovery. Indeed, various plasma metabolites and glycomic features of plasma glycoproteins have
285 been investigated as biomarkers for several diseases, including IBD, diabetes, cardiovascular
286 diseases, and cancer.[65-71] In addition, markers of intestinal barrier permeability have been used as
287 predictors of multiple organ dysfunction during critical illness.[72] The striking differences we
288 observed in the levels of specific metabolites, lipids, and glycoproteins between COVID-19
289 disease states suggests they may also have value for risk prediction or therapeutic response. Future
290 longitudinal, controlled studies will be needed to assess these possibilities.

291 Our study also reveals several potential therapeutic targets for severe COVID-19, including
292 zonulin. Zonulin is the only known physiological modulator of the intestinal tight junctions.[73]
293 Microbial dysbiosis and translocation enhance zonulin release, which in turn induces tight junction
294 permeability, leading to more microbial translocation. This microbial translocation triggers
295 inflammation, which promotes further gut leakiness.[40,41] Increased intestinal permeability and
296 serum zonulin levels have been observed during many inflammatory diseases, including Crohn's
297 disease and celiac disease.[74,75] Preventing zonulin-mediated increase in intestinal permeability by
298 a zonulin receptor antagonist AT1001 (larazotide acetate) decreased the severity and incidence of
299 several inflammation-associated diseases in pre-clinical and clinical studies.[76-82] The strikingly
300 high level of serum zonulin we observed during severe COVID-19, which were associated with
301 inflammation and mortality, raise the question of whether modulators of tight junction
302 permeability (such as with AT-1001) can lessen COVID-19 severity.

303 Another question is whether there is a genetic predisposition to intestinal barrier permeability and
304 COVID-19 severity. Zonulin is the uncleaved precursor to haptoglobin (HP).[73] There are two
305 common alleles for haptoglobin, HP1 and HP2. Individuals with the HP2 allele produce high levels
306 of zonulin, whereas individuals with the HP1 allele do not.[41] High-zonulin-producers (HP2 allele)
307 are more likely to develop IBD[83,84] and experience morbidity from inflammatory diseases.[85,86] The
308 worldwide frequency of each haptoglobin phenotype varies by region.[84,87] How the HP genotype
309 and zonulin polymorphisms[88] are linked to severe COVID-19 and associated mortality should be
310 the subject of future studies.

311 A second potential therapeutic target revealed by this work is citrulline. Citrulline levels were
312 reduced in both moderate and severe COVID-19, and the citrulline metabolism and biosynthesis
313 pathways were among the top metabolic pathways disrupted in severe COVID-19. Citrulline is an
314 intermediate in arginine metabolism,[89] and a marker of gut and enterocyte function.[25,90] Disrupted
315 citrulline metabolism, as we observed during severe COVID-19, has been associated with
316 microbial dysbiosis and dysregulated intestinal function.[91] In addition to its role as a biomarker,
317 citrulline has an important role in preserving gut barrier function. In an intestinal obstruction
318 mouse model, pretreatment with a citrulline-rich diet preserved gut barrier integrity.[92] Thus, our
319 data, and the work of others from diverse fields, suggest that greater understanding of the
320 interaction between the gut, intestinal microbiota, and amino acid metabolism during COVID-19
321 might inform pharmaceutical and diet approaches to improve COVID-19 outcomes.

322 A significant strength of our multi-omics approach is its ability to uncover connections between
323 severe COVID-19 and biomolecules of different classes. The carbohydrate structures (glycans)
324 attached to circulating proteins, including antibodies, and their receptors (lectins) are increasingly
325 being appreciated for their essential roles in a variety of immune functions. Among the
326 glycobiological molecules regulated by severe COVID-19 are galectins (increasing) and
327 galactosylated glycans on circulating glycoproteins (decreasing). Both may point to a potential
328 glycomic contributions to the severity of COVID-19. First, galectins (secreted, GalNAc-binding
329 proteins) have emerged as significant modulators of cytokine expression by immune cells during
330 several diseases, including viral infections.[93-95] Importantly, small molecule inhibitors for
331 galectins, especially for Gal-3, can reduce inflammation and cytokine release.[96,97] Therefore,
332 galectins represent potential therapeutic targets to reduce cytokine storm during COVID-19.[98,99]
333 Second, galactosylated glycans on circulating antibodies link Dectin-1 on phagocytes to FcγRIIB

334 on myeloid cells to prevent the inflammation mediated by complement activation.[31] Loss of
335 galactose, as observed during COVID-19, decreases the opportunity to activate this important anti-
336 complement activation checkpoint, thereby promoting inflammation. As using highly-
337 galactosylated immune complexes can prevent inflammation mediated by complement
338 activation,[31] these and similar glycomic approaches may represent another therapeutic opportunity
339 to reduce inflammation during COVID-19.

340 Caveats of our study include the sample size and sampling of blood. As noted above, correcting
341 for potential confounders will require larger cohorts from varying geographic and demographic
342 settings. Independent test sets and samples from non-COVID1-9 hospitalized and ICU-admitted
343 patients will also be needed. In addition, longitudinal analyses will be required to examine the
344 long-term implications of our findings and their potential value as prognostic biomarkers. Analysis
345 of gut biopsies, stool, and bronchial lavage will be needed to determine the precise contributions
346 of the gut-lung axis in COVID-19. Finally, mechanistic studies *in vitro* and in animal models of
347 SARS-CoV2 infection will be needed to examine the direct versus the indirect impact of the
348 infection on intestinal barrier integrity and function.

349 In summary, while this study was exploratory in nature, our data strongly suggest for the first time:
350 (1) severe COVID-19 is associated with disrupted intestinal barrier integrity, higher microbial
351 translocation, and gut dysfunction; (2) severe COVID-19 is associated with a dramatic shift in
352 levels of several biologically active molecules, which likely contribute to disease severity by
353 inducing inflammation. Our study is beginning to shed light on the potentially critical role of a
354 previously unappreciated factor, disruption of intestinal barrier integrity, in the pathophysiology
355 of severe COVID-19. By understanding these unappreciated underpinnings of COVID-19, this
356 work may serve to identify biomarkers for risk stratification and build a foundation for developing
357 strategies to prevent or reduce the severity of COVID-19.

358 **METHODS**

359 ***Study cohort.*** Analyses were performed using plasma samples from 60 individuals tested positive
360 for SARS-CoV2, and 20 SARS-CoV2 negative controls collected at Rush University Medical
361 Center (RUMC). The 60 SARS-CoV2 positives were selected to represent three diseases states:
362 20 with mild symptoms (outpatients); 20 with moderate symptoms (inpatients hospitalized on
363 regular wards); and 20 with severe symptoms (inpatients hospitalized in an intensive care unit
364 (ICU)) (**Figure 1a**). Individuals were selected to have a median age between 52.5 to 58.5 years.
365 The study cohort was also chosen to have a 35 to 60% representation of female gender per disease
366 status group (**Supplementary Table 1**). Eight participants of the cohort (two from the moderate
367 group and six from the severe group) died from COVID-19 (**Supplementary Table 1**). All
368 research protocols of the study were approved by the institutional review boards (IRB) at Rush
369 University and The Wistar Institute. All human experimentation was conducted in accordance with
370 the guidelines of the US Department of Health and Human Services and those of the authors'
371 institutions.

372 ***Measurement of plasma markers of tight junction permeability and microbial translocation.***
373 Plasma levels of soluble CD14 (sCD14), soluble CD163 (sCD163), LPS Binding Protein (LBP),
374 and FABP2/I-FABP were quantified using DuoSet ELISA kits (R&D Systems; catalog # DY383-
375 05, # DY1607-05, # DY870-05, and # DY3078, respectively). The plasma level of zonulin was
376 measured using an ELISA kit from MyBiosorce (catalog # MBS706368). Levels of occludin were
377 measured by ELISA (Biomatik; catalog # EKC34871). β-glucan detection in plasma was
378 performed using Limulus Amebocyte Lysate (LAL) assay (Glucatell Kit, CapeCod; catalog #
379 GT003). Plasma levels of Reg3A were measured by ELISA (RayBiotech; catalog # ELH-REG3A-
380 1).

381 ***Measurement of plasma markers of inflammation and immune activation.*** Plasma levels of GM-
382 CSF, IFN-β, IFN-γ, IL-10, IL-13, IL-1β, IL-33, IL-4, IL-6, TNF-α, Fractalkine, IL-12p70, IL-2,
383 IL-21, IL-22, IL-23, IP-10, MCP-2, MIP-1α, SDF-1a, IFN-α2a, IL-12/IL-23p40, and IL-15 were
384 determined using customized MSD U-PLEX multiplex assay (Meso Scale Diagnostic catalog#
385 K15067L-2). Plasma levels of C-Reactive Protein (CRP), Galectin-1, Galectin-3, and Galectin-9
386 were measured using DuoSet ELISA kits (R&D Systems; catalog # DY1707, # DY1152-05, #

387 DY2045, and # DY1154, respectively). Levels of Growth Differentiation Factor-15 (GDF-15)
388 were measured by ELISA using GDF-15 Quantikine ELISA Kit (R&D Systems; catalog #
389 DGD150). Plasma levels of Myeloperoxidase (MPO), d-dimer, and C3a were measured by ELISA
390 (Thermo Fischer; catalog # BMS2038INST, # EHDDIMER, #BMS2089, respectively)

391 ***Untargeted measurement of plasma metabolites.*** Metabolomics analysis was performed as
392 described previously.[100] Briefly, polar metabolites were extracted from plasma samples with 80%
393 methanol. A quality control (QC) sample was generated by pooling equal volumes of all samples
394 and was injected periodically during the analysis sequence. LC-MS/MS was performed on a
395 Thermo Scientific Q Exactive HF-X mass spectrometer with HESI II probe and Vanquish Horizon
396 UHPLC system. Hydrophilic interaction liquid chromatography was performed at 0.2 ml/min on
397 a ZIC-pHILIC column (2.1 mm × 150 mm, EMD Millipore) at 45°C. Solvent A was 20 mM
398 ammonium carbonate, 0.1% ammonium hydroxide, pH 9.2, and solvent B was acetonitrile. The
399 gradient was 85% B for 2 min, 85% B to 20% B over 15 min, 20% B to 85% B over 0.1 min, and
400 85% B for 8.9 min. All samples were analyzed by full MS with polarity switching. The QC sample
401 was also analyzed by data-dependent MS/MS with separate runs for positive and negative ion
402 modes. Full MS scans were acquired at 120,000 resolution with a scan range of 65-975 m/z. Data-
403 dependent MS/MS scans were acquired for the top 10 highest intensity ions at 15,000 resolution
404 with an isolation width of 1.0 m/z and stepped normalized collision energy of 20-40-60. Data
405 analysis was performed using Compound Discoverer 3.1 (ThermoFisher Scientific). Metabolites
406 were identified by accurate mass and retention time using an in-house database generated from
407 pure standards or by MS2 spectra using the mzCloud spectral database (mzCloud.org) and
408 selecting the best matches with scores of 50 or greater. Metabolite quantification used peak areas
409 from full MS runs and were corrected based on the periodic QC runs.

410 ***Untargeted measurement of plasma lipids.*** Lipidomics analysis was performed as described
411 previously.[101] Briefly, plasma samples were spiked with EquiSplash mix (Avanti Polar Lipids).
412 Lipids were extracted with 2:1:1 chloroform: methanol: 0.8% sodium chloride. Samples were
413 resuspended in 1:9 chloroform: methanol after drying the organic phase under nitrogen. LC-MS
414 runs were performed on a Thermo Scientific Q Exactive HF-X mass spectrometer with HESI II
415 probe and Vanquish Horizon UHPLC system. Reversed-phase liquid chromatography was
416 performed at 0.35 ml/min on an Accucore C30 column (2.1 mm x 150 mm, ThermoFisher

417 Scientific) at 50°C. Solvent A was 50:50 acetonitrile: water, and solvent B was 88:10:2
418 isopropanol: acetonitrile: water solvents. Both solvents contained 5 mM ammonium formate and
419 0.1% formic acid. The gradient was 0% B for 3 min, 0% to 60% B over 7 min, 60% to 85% B over
420 10 min, 85% to 100% B over 10 min, 100% B for 5 min, 100% to 0% B over 0.01 min, and 0% B
421 for 4.99 min. All samples were analyzed by data-dependent MS/MS with separate runs for positive
422 and negative ion modes. Full MS scans were acquired at 120,000 resolution with a scan range of
423 300-2,000 m/z in positive mode and 250-2,000 m/z in negative mode. Data-dependent MS/MS
424 scans were acquired for the top 20 ions at 15,000 resolution with an isolation width of 0.4 m/z.
425 Stepped normalized collision energy of 20-30 was used for positive ion mode and 20-30-40 was
426 used for negative ion mode. Data analysis was performed using LipidSearch 4.2 (ThermoFisher
427 Scientific). Lipid species were identified from MS/MS spectra using an in-silico fragmentation
428 database and were filtered by expected adducts and identification quality. Lipid species
429 quantification used peak areas and was corrected based on EquiSplash deuterated lipids for
430 represented classes.

431 ***IgG isolation.*** Bulk IgG was purified from plasma using Pierce Protein G Spin Plate (Thermo
432 Fisher; catalog # 45204). IgG purity was confirmed by SDS gel.

433 ***IgA isolation.*** Bulk IgA was purified from IgG depleted plasma using CaptureSelect IgA Affinity
434 Matrix (Thermo Fisher; catalog # 194288010). IgA was concentrated using Amicon® filters
435 (Milipore catalogue #UFC805024) and purity was confirmed by SDS gel.

436 ***N-glycan analysis using capillary electrophoresis.*** For both plasma and bulk IgG, *N*-glycans were
437 released using peptide-N-glycosidase F (PNGase F) and labeled with 8-aminopyrene-1,3,6-
438 trisulfonic acid (APTS) using the GlycanAssure APTS Kit (Thermo Fisher; catalog # A33952),
439 following the manufacturer's protocol. Labeled *N*-glycans were analyzed using the 3500 Genetic
440 Analyzer capillary electrophoresis system. Total plasma *N*-glycans were separated into 24 peaks
441 (**Supplementary Table 6**) and IgG *N*-glycans into 22 peaks (**Supplementary Table 7**). The
442 relative abundance of *N*-glycan structures was quantified by calculating the area under the curve
443 of each glycan structure divided by the total glycans using the Applied Biosystems GlycanAssure
444 Data Analysis Software Version 2.0.

445 ***Glycan analysis using lectin array.*** To profile plasma total and IgA glycomes, we used the lectin
446 microarray as it enables analysis of multiple glycan structures. The lectin microarray employs a
447 panel of 45 immobilized lectins with known glycan-binding specificity (lectins and their glycan-
448 binding specificity are detailed in **Supplementary Table 8**). Plasma proteins or isolated IgA were
449 labeled with Cy3 and hybridized to the lectin microarray. The resulting chips were scanned for
450 fluorescence intensity on each lectin-coated spot using an evanescent-field fluorescence scanner
451 GlycoStation Reader (GlycoTechnica Ltd.), and data were normalized using the global
452 normalization method.

453 ***Statistical analysis.*** Kruskal-Wallis and Mann–Whitney U tests were used for unpaired
454 comparisons. Spearman's rank correlations were used for bivariate correlation analyses. Severity
455 correlation coefficient (SC *rho*) tested correlation versus patient groups with the severity groups
456 quantified as follows: control=1, mild=2, moderate=3, severe=4. FDR for each type of comparison
457 was calculated using the Benjamini–Hochberg approach within each data subset separately and
458 FDR<5% was used as a significance threshold. Principal Component Analysis was performed on
459 log2-transcformed z-scored data. Pathway enrichment analyses were done on features that passed
460 significant SC *rho* at FDR<5%. Enrichments for the metabolites were tested using QIAGEN's
461 Ingenuity® Pathway Analysis software (IPA®, QIAGEN Redwood City,
462 www.qiagen.com/ingenuity) using the "Canonical Pathway" option. Enrichments for the lipids
463 were done using LIPEA (https://lipea.biotec.tu-dresden.de/home) with default parameters. To
464 explore biomarkers that could be distinguish clinical outcome (hospitalization vs. non-
465 hospitalization), specific set of microbial translocation variables were identified among those with
466 FDR<0.05. Variables for the multivariable logistic model were selected from the identified
467 specific set of biomarkers using Lasso technique with the cross-validation (CV) selection option
468 by separating data in 5-fold. Due to the exploratory nature of this study with moderate sample size,
469 variable selection was determined using 100 independent rounds runs of CV Lasso with minimum
470 tuning parameter lambda. The markers that were selected 80 or more times from 100 runs were
471 used as final set of variables in our model. The ability of the final logistic model was assessed by
472 AUC with 95% confidence interval. Statistical analyses were performed in R 4.0.2 and Prism 7.0
473 (GraphPad).

FIGURE LEGENDS

Figure 1. Severe COVID-19 is associated with an increase in markers of tight junction permeability and microbial translocation. (a) An overview of the study design; figures in black indicate deceased; moderate and severe patients were hospitalized; severe indicates patients in the intensive care unit. **(b)** Levels of plasma zonulin, a marker of tight junction permeability, are higher during moderate and severe COVID-19 compared to mild COVID-19 or controls. Kruskal–Wallis test was used for statistical analysis. False discovery rate (FDR) was calculated using the Benjamini-Hochberg method. Symbols in black indicate deceased. **(c)** Zonulin levels are higher in hospitalized COVID patients (n=40) who eventually died from COVID-19 (n=8) compared to survivors (n=32). Nominal *P*-value was calculated using the Mann–Whitney U test. **(d-g)** Levels of markers of translocation and inflammation, LBP **(d)**, β-Glucan **(e)**, sCD14 **(f)**, and MPO **(g)**, are higher during severe COVID-19 compared to mild COVID-19 or controls. Kruskal–Wallis test was used for statistical analysis. FDR was calculated using Benjamini-Hochberg method.

Figure 2. Markers of tight junction permeability and microbial translocation are linked to systemic inflammation and immune dysfunction. (a left) Heat-map depicting plasma levels of 23 inflammation and immune activation/dysfunction markers whose levels are statistically (FDR<0.05) different between the four disease states. Statistical significance was determined using the Kruskal–Wallis test. FDR was calculated using Benjamini-Hochberg method. SC *rho* = coefficient of correlation with COVID-19 severity. Heat colors show standardized Z-scores across samples; red indicates upregulation and blue indicates downregulation. **(a right)** Coefficients of correlation between zonulin, LBP, or β-Glucan and each of the 23 inflammation and immune activation/dysfunction markers. All red-colored correlations had statistical significance of FDR<0.05, whereas the grey-colored correlation was non-significant. Correlations were evaluated using Spearman's rank correlation tests, and FDR was calculated using the Benjamini-Hochberg method. **(b-d)** Levels of representative variables, galectin-3 (Gal-3) **(b)** and galectin-9 (Gal-9) **(c),** were higher during severe COVID-19 compared to mild COVID-19 or controls, with levels of Gal-9 higher among deceased hospitalized patients compared to survivors **(d)**. **(e-g)** Levels of C3a **(e)** and GDF-15 **(f)** were higher during severe COVID-19 compared to mild COVID-19 or controls, with levels of GDF-15 higher among deceased hospitalized patients compared to survivors **(g)**. Kruskal–Wallis and Mann-Whitney tests were used for statistical analysis. FDR was

calculated using Benjamini-Hochberg method. **(h-i)** Examples of correlations in (a) between LBP and IL-6 **(h)** or β-Glucan and IL-6 **(i)**. Spearman's rank correlation tests were used for statistical analysis.

Figure 3. Severe COVID-19 is associated with metabolic dysregulation in a manner linked to gut dysfunction. (a) Principal component analysis (PCA) of the 278 metabolites identified in the plasma of the study cohort. Each symbol represents a study participant. **(b)** Ingenuity Pathway Analysis (IPA) of the plasma metabolites modulated between the disease states with FDR<0.05. The graph shows the top 10 dysregulated metabolic pathways with FDR<0.05. Percentages beside each pathway represent the ratio of dysregulated metabolites among the total number of metabolites assigned to this particular pathway in IPA. **(c)** Volcano plots depicting plasma metabolites dysregulated in the moderate group compared to the mild group (left) or the severe group compared to the mild group (right). NS= non-significant. The gut-associated metabolites (from Table 1) are indicated by the larger symbols, and a selected set are identified by name. **(d-f)** As representative examples, levels of Citrulline are lower **(d)**, levels of succinic acid are higher **(e)**, and the ratio between kynurenine/tryptophan [Kyn/Trp] is higher **(f)** during severe COVID-19 compared to mild COVID-19 or controls. Kruskal–Wallis test was used for statistical analysis. FDR was calculated using Benjamini-Hochberg method. **(g-h)** For key metabolites in the tryptophan catabolism pathway, levels of tryptophan are lower **(g)**, and levels of kynurenic acid are higher **(h)** in deceased COVID-19 hospitalized patients compared to survivors. Nominal *P*-value was calculated using the Mann–Whitney U test.

Figure 4. Metabolic markers of intestinal dysfunction are linked to microbial translocation and systemic inflammation. Correlation heat-maps depicting the correlations between COVID-19-modulated, gut-associated metabolites and **(a)** markers of tight junction permeability and microbial translocation or (**b**) markers of inflammation and immune dysfunction. SC *rho* = coefficient of correlation with COVID-19 severity. Red-colored correlations = positive correlations with FDR<0.05, blue-colored correlations = negative correlations with FDR<0.05, gray-colored correlations = non-significant (FDR>0.05). **(c-e)** Examples of the correlations between citrulline and IL-6 **(c)**, succinic acid and IL-6 **(d),** or [Kyn/Trp] ratio and IL-6 **(e)**. Spearman's rank correlation tests were used for statistical analysis. FDR was calculated using Benjamini-Hochberg method.

Figure 5. Severe COVID-19 is associated with disrupted lipid metabolism. (a) Principal component analysis (PCA) of 2015 lipids identified in the plasma of the study cohort. **(b)** The 2015 identified lipids were assigned to 24 classes (Supplementary Table 5). Heat-map depicts the 16 lipid classes dysregulated by severe COVID-19 (FDR<0.05). Statistical significance was determined using the Kruskal–Wallis test. FDR was calculated using Benjamini-Hochberg method. SC *rho* = coefficient of correlation with COVID-19 severity. Heat colors show standardized Z-scores across samples; red indicates upregulation, and blue indicates downregulation. **(c)** Lipid pathway analysis of the plasma lipids modulated between the disease states with FDR<0.05 was performed using LIPEA (Lipid Pathway Enrichment Analysis; https://lipea.biotec.tu-dresden.de/home). The graph includes all dysregulated pathways with FDR<0.05. Percentages beside each pathway represent the ratio of dysregulated lipids among the total number of lipids assigned to this particular pathway by LIPEA.

Figure 6. Severe COVID-19 is associated with plasma glycomic dysregulations. (a) Heat-map depicting glycans dysregulated by severe COVID-19 (FDR<0.05). Names of the glycan-binding lectins are provided in parentheses. Statistical significance was determined using the Kruskal–Wallis test. FDR was calculated using Benjamini-Hochberg method. SC *rho* = coefficient of correlation with COVID-19 severity. Heat colors show standardized Z-scores across samples; red indicates upregulation, and blue indicates downregulation. **(b-c)** Levels of terminal digalactosylated *N*-glycans in IgG **(b)** or total plasma glycoproteins **(c)** are lower during severe COVID-19 compared to mild COVID-19 or controls. Kruskal–Wallis test. FDR was calculated using Benjamini-Hochberg method. **(e-d)** Correlation heat-maps depicting the correlations between galactosylated *N*-glycans (rows) and markers of tight junction permeability and microbial translocation **(d)** or markers of inflammation and immune dysfunction (**e**). SC *rho* = coefficient of correlation with COVID-19 severity. Red-colored correlations = positive correlations with FDR<0.05, blue-colored correlations = negative correlations with FDR<0.05, and gray-colored correlations = non-significant. Spearman's rank correlation tests were used for statistical analysis. FDR was calculated using Benjamini-Hochberg method.

Figure 7. Logistic models using markers of tight-junction permeability and microbial translocation strongly distinguish hospitalized from non-hospitalized individuals. **(a)** The machine learning algorithm, Lasso (least absolute shrinkage and selection operator) regularization,

selected three markers (zonulin, LBP, and sCD14) that, when combined, can distinguish hospitalized (n=40; severe and moderate groups combined) from non-hospitalized (n=40; mild and control groups combined) individuals. The receiver operator characteristic (ROC) curve showing an area under the curve (AUC) of 99.23% from the multivariable logistic regression model with the three variables combined. (**B**) Coefficients from the multivariable logistic model were used to estimate a hospitalization risk score for each individual and then tested for the ability of these scores to accurately classify hospitalized (n=40) from non-hospitalized (n=39; one sample did not have a complete dataset) individuals at an optimal cut-point. The model correctly classified hospitalized (97.5% sensitivity) and non-hospitalized (94.9% specificity), with an overall accuracy of 96.2%. Squares represent individuals the model failed to identify correctly. **(c)** Logistic regression model using the L-kynurenine/L-tryptophan [Kyn/Trp] ratio, a marker of gut microbiome dysbiosis, is able to distinguish hospitalized from non-hospitalized individuals. ROC curve showing the area under the curve (AUC) is 91.3%.

TABLES

Table 1. Levels of the 35 (out of 50) gut- and gut microbiota-associated plasma metabolites that are disrupted during COVID-19. Red indicates upregulation, blue indicates downregulation; color intensity indicates larger difference. Green indicates FDR<0.05; color intensity indicates lower FDR.

Table 2. Results of logistic regression models of tight junction permeability and microbial translocation markers for ability to distinguish hospitalized from non-hospitalized individuals.

SUPPLEMENTARY MATERIALS

Supplementary Figure 1: Top 50 metabolites dysregulated by COVID-19. Heat-maps depicting the top 25 metabolites induced and the top 25 metabolites reduced by COVID-19 (FDR<0.05). Statistical significance was determined using the Kruskal–Wallis test. FDR was calculated using Benjamini-Hochberg method. SC *rho* = coefficient of correlation with COVID-

19 severity. Heat colors show standardized Z-scores across samples; red indicates upregulation, and blue indicates downregulation.

Supplementary Figure 2: The COVID-19-associated plasma glycomic signatures are associated with microbial translocation and systemic inflammation. Correlation heat-maps depicting the correlations between COVID-19 modulated plasma glycans and **(a)** markers of tight junction permeability and microbial translocation or (**b**) markers of inflammation and immune dysfunction. SC *rho* = coefficient of correlation with COVID-19 severity. Red-colored correlations = positive correlations with FDR<0.05, blue-colored correlations = negative correlations with FDR<0.05, and gray-colored correlations = non-significant correlations.

Supplementary Table 1. Demographic and clinical characteristics of the study cohort.

Supplementary Table 2: A list of plasma markers measured in this study.

Supplementary Table 3: Top 50 metabolic pathways disrupted by severe COVID-19.

Supplementary Table 4: List of the gut-associated and gut microbiota-associated metabolites detected in our study using untargeted LC-MS/MS (50 of the 278 metabolites identified in plasma).

Supplementary Table 5. The two thousand fifteen lipids identified in this study were assigned to 24 lipid classes.

Supplementary Table 6. The structures and names of *N*-glycans identified in plasma by capillary electrophoresis. These glycan structures can be grouped into 15 groups: bisecting GlcNAc (B group), sialic acid (non-siaylated (S0), mono-sialylated (S1), di-sialylated (S2), tri-sialylatedand (S3), tetra-sialylated (S4), and total sialylated (ST)), galactose (agalactosylated (G0), mono-galactosylated (G1), di-galactosylated (G2), and total galactosylated (GT)), core fucose (FC group), branched fucose (FB group), high branched (HB group), and low branch (LB group).

Supplementary Table 7. The structures and names of *N*-glycans identified in IgG by capillary electrophoresis. These glycan structures were grouped into 9 groups, depending on the presence or absence of four key monosaccharides: bisecting GlcNAc (B group), sialic acid (mon-sialylated (S1), di-sialylated (S2), and total siaylated (ST)), terminal galactose (agalactosylated (G0), mono-galactosylated (G1), di-galactosylated (G2), and total galactose (GT)), and fucose (F group).

Supplementary Table 8. Lectins used in the 45-plex lectin microarray and their glycan-binding specificity.

AUTHOR CONTRIBUTIONS

M.A-M, A.L, and A.Ke conceived and designed the study. L.B.G. carried out the majority of experiments. H.D., X.Y, H.W, Q.L, and A.Ko performed all bioinformatics and biostatistical analyses. M.D. ran the lectin array experiments. C.S.P reviewed and selected gut-associated metabolites. N.F.Z, R.A.B, M.W.S, CBF, A.Ke, and A.L selected study participants and interpreted data. A.R.G, N.G, and H.T performed metabolic and lipidomic analyses. L.B.G. and M.A-M wrote the manuscript, and all authors edited it.

ACKNOWLEDGMENTS

This study is supported by a supplement to R01 DK123733 (R01 DK123733-01S1) for M.A-M, A.L, and A.Ke and R24 AA026801- 02S1 for A.Ke. M.A-M is also supported by The Foundation for AIDS Research (amfAR) impact grant # 109840-65-RGR, NIH grants (R01 AG062383, R01NS117458, R21 AI143385, R21 AI129636, and R21 NS106970), and the Penn Center for AIDS Research (P30 AI 045008). The Wistar Proteomics and Metabolomics Shared Resource is supported in part by NIH Cancer Center Support Grant CA010815. The Thermo Q-Exactive HF-X mass spectrometer was purchased with NIH grant S10 OD023586. We would like to thank Rachel E. Locke, Ph.D. for providing comments.

COMPETING INTERESTS STATEMENT

The authors have no competing interests.

REFERENCES

1. Guan, W.J., *et al.* Clinical Characteristics of Coronavirus Disease 2019 in China. *The New England journal of medicine* **382**, 1708-1720 (2020).

2. Gandhi, R.T., Lynch, J.B. & Del Rio, C. Mild or Moderate Covid-19. *The New England journal of medicine* (2020).

3. Grasselli, G., *et al.* Baseline Characteristics and Outcomes of 1591 Patients Infected With SARS-CoV-2 Admitted to ICUs of the Lombardy Region, Italy. *Jama* **323**, 1574-1581 (2020).

4. Richardson, S., *et al.* Presenting Characteristics, Comorbidities, and Outcomes Among 5700 Patients Hospitalized With COVID-19 in the New York City Area. *Jama* **323**, 2052-2059 (2020).

5. Chen, N., *et al.* Epidemiological and clinical characteristics of 99 cases of 2019 novel coronavirus pneumonia in Wuhan, China: a descriptive study. *Lancet* **395**, 507-513 (2020).

6. Blanco-Melo, D., *et al.* Imbalanced Host Response to SARS-CoV-2 Drives Development of COVID-19. *Cell* **181**, 1036-1045 e1039 (2020).

7. Chen, G., *et al.* Clinical and immunological features of severe and moderate coronavirus disease 2019. *The Journal of clinical investigation* **130**, 2620-2629 (2020).

8. Mehta, P., *et al.* COVID-19: consider cytokine storm syndromes and immunosuppression. *Lancet* **395**, 1033-1034 (2020).

9. Huang, C., *et al.* Clinical features of patients infected with 2019 novel coronavirus in Wuhan, China. *Lancet* **395**, 497-506 (2020).

10. Risitano, A.M., *et al.* Complement as a target in COVID-19? *Nature reviews. Immunology* (2020).

11. Dumas, A., Bernard, L., Poquet, Y., Lugo-Villarino, G. & Neyrolles, O. The role of the lung microbiota and the gut-lung axis in respiratory infectious diseases. *Cellular microbiology* **20**, e12966 (2018).

12. Frati, F., *et al.* The Role of the Microbiome in Asthma: The Gut(-)Lung Axis. *International journal of molecular sciences* **20**(2018).

13. Mukherjee, S. & Hanidziar, D. More of the Gut in the Lung: How Two Microbiomes Meet in ARDS. *Yale J Biol Med* **91**, 143-149 (2018).

14. Dickson, R.P.*, et al.* Enrichment of the lung microbiome with gut bacteria in sepsis and the acute respiratory distress syndrome. *Nat Microbiol* **1**, 16113 (2016).

15. Lamers, M.M.*, et al.* SARS-CoV-2 productively infects human gut enterocytes. *Science* (2020).

16. Brenchley, J.M.*, et al.* CD4+ T cell depletion during all stages of HIV disease occurs predominantly in the gastrointestinal tract. *J. Exp. Med.* **200**, 749-759 (2004).

17. Niessen, C.M. Tight junctions/adherens junctions: basic structure and function. *The Journal of investigative dermatology* **127**, 2525-2532 (2007).

18. Turner, J.R. Intestinal mucosal barrier function in health and disease. *Nature reviews. Immunology* **9**, 799-809 (2009).

19. O'Toole, P.W. & Jeffery, I.B. Gut microbiota and aging. *Science* **350**, 1214-1215 (2015).

20. Thevaranjan, N.*, et al.* Age-Associated Microbial Dysbiosis Promotes Intestinal Permeability, Systemic Inflammation, and Macrophage Dysfunction. *Cell host & microbe* **21**, 455-466 e454 (2017).

21. Kim, K.A., Jeong, J.J., Yoo, S.Y. & Kim, D.H. Gut microbiota lipopolysaccharide accelerates inflamm-aging in mice. *BMC microbiology* **16**, 9 (2016).

22. Fransen, F.*, et al.* Aged Gut Microbiota Contributes to Systemical Inflammaging after Transfer to Germ-Free Mice. *Frontiers in immunology* **8**, 1385 (2017).

23. Zhang, C.*, et al.* Structural modulation of gut microbiota in life-long calorie-restricted mice. *Nature communications* **4**, 2163 (2013).

24. Klingelhoefer, L. & Reichmann, H. Pathogenesis of Parkinson disease--the gut-brain axis and environmental factors. *Nat Rev Neurol* **11**, 625-636 (2015).

25. Fragkos, K.C. & Forbes, A. Citrulline as a marker of intestinal function and absorption in clinical settings: A systematic review and meta-analysis. *United European Gastroenterol J* **6**, 181-191 (2018).

26. Fujisaka, S.*, et al.* Diet, Genetics, and the Gut Microbiome Drive Dynamic Changes in Plasma Metabolites. *Cell Rep* **22**, 3072-3086 (2018).

27. Kurilshikov, A., *et al.* Gut Microbial Associations to Plasma Metabolites Linked to Cardiovascular Phenotypes and Risk. *Circ Res* **124**, 1808-1820 (2019).

28. Mayneris-Perxachs, J. & Fernandez-Real, J.M. Exploration of the microbiota and metabolites within body fluids could pinpoint novel disease mechanisms. *FEBS J* **287**, 856-865 (2020).

29. Davaatseren, M., *et al.* Poly-gamma-glutamic acid attenuates angiogenesis and inflammation in experimental colitis. *Mediators Inflamm* **2013**, 982383 (2013).

30. Villeda-Gonzalez, J.D., *et al.* Nicotinamide reduces inflammation and oxidative stress via the cholinergic system in fructose-induced metabolic syndrome in rats. *Life Sci* **250**, 117585 (2020).

31. Karsten, C.M., *et al.* Anti-inflammatory activity of IgG1 mediated by Fc galactosylation and association of FcgammaRIIB and dectin-1. *Nature medicine* **18**, 1401-1406 (2012).

32. Cao, Y., Rocha, E.R. & Smith, C.J. Efficient utilization of complex N-linked glycans is a selective advantage for Bacteroides fragilis in extraintestinal infections. *Proceedings of the National Academy of Sciences of the United States of America* **111**, 12901-12906 (2014).

33. Simurina, M., *et al.* Glycosylation of Immunoglobulin G Associates With Clinical Features of Inflammatory Bowel Diseases. *Gastroenterology* **154**, 1320-1333 e1310 (2018).

34. Bamba, T., Matsuda, H., Endo, M. & Fujiyama, Y. The pathogenic role of Bacteroides vulgatus in patients with ulcerative colitis. *J Gastroenterol* **30 Suppl 8**, 45-47 (1995).

35. Huang, Y.L., Chassard, C., Hausmann, M., von Itzstein, M. & Hennet, T. Sialic acid catabolism drives intestinal inflammation and microbial dysbiosis in mice. *Nature communications* **6**, 8141 (2015).

36. Matsuda, H., *et al.* Characterization of antibody responses against rectal mucosa-associated bacterial flora in patients with ulcerative colitis. *J Gastroenterol Hepatol* **15**, 61-68 (2000).

37. Bloom, S.M., *et al.* Commensal Bacteroides species induce colitis in host-genotype-specific fashion in a mouse model of inflammatory bowel disease. *Cell host & microbe* **9**, 390-403 (2011).

38. Monaghan, T.M., *et al.* Decreased Complexity of Serum N-glycan Structures Associates with Successful Fecal Microbiota Transplantation for Recurrent Clostridioides difficile Infection. *Gastroenterology* **157**, 1676-1678 e1673 (2019).

39. Fasano, A. Zonulin and its regulation of intestinal barrier function: the biological door to inflammation, autoimmunity, and cancer. *Physiol Rev* **91**, 151-175 (2011).

40. El Asmar, R.*, et al.* Host-dependent zonulin secretion causes the impairment of the small intestine barrier function after bacterial exposure. *Gastroenterology* **123**, 1607-1615 (2002).

41. Wood Heickman, L.K., DeBoer, M.D. & Fasano, A. Zonulin as a potential putative biomarker of risk for shared type 1 diabetes and celiac disease autoimmunity. *Diabetes Metab Res Rev* **36**, e3309 (2020).

42. Muta, T. & Takeshige, K. Essential roles of CD14 and lipopolysaccharide-binding protein for activation of toll-like receptor (TLR)2 as well as TLR4 Reconstitution of TLR2- and TLR4-activation by distinguishable ligands in LPS preparations. *Eur J Biochem* **268**, 4580-4589 (2001).

43. Morris, A.*, et al.* Serum (1-->3)-beta-D-glucan levels in HIV-infected individuals are associated with immunosuppression, inflammation, and cardiopulmonary function. *Journal of acquired immune deficiency syndromes* **61**, 462-468 (2012).

44. Isnard, S.*, et al.* Plasma Levels of C-Type Lectin REG3alpha and Gut Damage in People With Human Immunodeficiency Virus. *The Journal of infectious diseases* **221**, 110-121 (2020).

45. Whitt, D.D. & Demoss, R.D. Effect of microflora on the free amino acid distribution in various regions of the mouse gastrointestinal tract. *Appl Microbiol* **30**, 609-615 (1975).

46. Ma, N. & Ma, X. Dietary Amino Acids and the Gut-Microbiome-Immune Axis: Physiological Metabolism and Therapeutic Prospects. *Compr Rev Food Sci F* **18**, 221-242 (2019).

47. Blachier, F., Mariotti, F., Huneau, J.F. & Tome, D. Effects of amino acid-derived luminal metabolites on the colonic epithelium and physiopathological consequences. *Amino acids* **33**, 547-562 (2007).

48. Schaible, U.E. & Kaufmann, S.H. A nutritive view on the host-pathogen interplay. *Trends in microbiology* **13**, 373-380 (2005).

49. Mellor, A.L. & Munn, D.H. IDO expression by dendritic cells: tolerance and tryptophan catabolism. *Nature reviews. Immunology* **4**, 762-774 (2004).

50. Vujkovic-Cvijin, I.*, et al.* Dysbiosis of the gut microbiota is associated with HIV disease progression and tryptophan catabolism. *Sci Transl Med* **5**, 193ra191 (2013).

51. Zhao, M., *et al.* Modulation of the Gut Microbiota during High-Dose Glycerol Monolaurate-Mediated Amelioration of Obesity in Mice Fed a High-Fat Diet. *mBio* **11**(2020).

52. Wahlstrom, A., Sayin, S.I., Marschall, H.U. & Backhed, F. Intestinal Crosstalk between Bile Acids and Microbiota and Its Impact on Host Metabolism. *Cell Metab* **24**, 41-50 (2016).

53. Liang, W., *et al.* Alterations Of Glycerophospholipid And Fatty Acyl Metabolism In Multiple Brain Regions Of Schizophrenia Microbiota Recipient Mice. *Neuropsychiatr Dis Treat* **15**, 3219-3229 (2019).

54. Ehehalt, R., *et al.* Phosphatidylcholine and lysophosphatidylcholine in intestinal mucus of ulcerative colitis patients. A quantitative approach by nanoElectrospray-tandem mass spectrometry. *Scand J Gastroenterol* **39**, 737-742 (2004).

55. Tateno, H., Kuno, A., Itakura, Y. & Hirabayashi, J. A versatile technology for cellular glycomics using lectin microarray. *Methods in enzymology* **478**, 181-195 (2010).

56. Mao, R., *et al.* Manifestations and prognosis of gastrointestinal and liver involvement in patients with COVID-19: a systematic review and meta-analysis. *Lancet Gastroenterol Hepatol* **5**, 667-678 (2020).

57. Pan, L., *et al.* Clinical Characteristics of COVID-19 Patients With Digestive Symptoms in Hubei, China: A Descriptive, Cross-Sectional, Multicenter Study. *Am J Gastroenterol* **115**, 766-773 (2020).

58. Livanos, A.E., *et al.* Gastrointestinal involvement attenuates COVID-19 severity and mortality. *medRxiv*, 2020.2009.2007.20187666 (2020).

59. Ngai, J.C., *et al.* The long-term impact of severe acute respiratory syndrome on pulmonary function, exercise capacity and health status. *Respirology* **15**, 543-550 (2010).

60. Wu, Q., *et al.* Altered Lipid Metabolism in Recovered SARS Patients Twelve Years after Infection. *Scientific reports* **7**, 9110 (2017).

61. Vyboh, K., Jenabian, M.A., Mehraj, V. & Routy, J.P. HIV and the gut microbiota, partners in crime: breaking the vicious cycle to unearth new therapeutic targets. *Journal of immunology research* **2015**, 614127 (2015).

62. Vazquez-Castellanos, J.F., *et al.* Altered metabolism of gut microbiota contributes to chronic immune activation in HIV-infected individuals. *Mucosal Immunol* **8**, 760-772 (2015).

63. Dinh, D.M., *et al.* Intestinal microbiota, microbial translocation, and systemic inflammation in chronic HIV infection. *J Infect Dis* **211**, 19-27 (2015).

64. Knoop, K.A., McDonald, K.G., Kulkarni, D.H. & Newberry, R.D. Antibiotics promote inflammation through the translocation of native commensal colonic bacteria. *Gut* **65**, 1100-1109 (2016).

65. Brindle, J.T., *et al.* Rapid and noninvasive diagnosis of the presence and severity of coronary heart disease using 1H-NMR-based metabonomics. *Nat Med* **8**, 1439-1444 (2002).

66. Oeckl, P. & Otto, M. A Review on MS-Based Blood Biomarkers for Alzheimer's Disease. *Neurol Ther* **8**, 113-127 (2019).

67. Hennig, R., *et al.* Towards personalized diagnostics via longitudinal study of the human plasma N-glycome. *Biochim Biophys Acta* **1860**, 1728-1738 (2016).

68. Keser, T., *et al.* Increased plasma N-glycome complexity is associated with higher risk of type 2 diabetes. *Diabetologia* **60**, 2352-2360 (2017).

69. Trbojevic Akmacic, I., *et al.* Inflammatory bowel disease associates with proinflammatory potential of the immunoglobulin G glycome. *Inflamm Bowel Dis* **21**, 1237-1247 (2015).

70. Vuckovic, F., *et al.* IgG Glycome in Colorectal Cancer. *Clinical cancer research : an official journal of the American Association for Cancer Research* **22**, 3078-3086 (2016).

71. Akinkuolie, A.O., Buring, J.E., Ridker, P.M. & Mora, S. A novel protein glycan biomarker and future cardiovascular disease events. *Journal of the American Heart Association* **3**, e001221 (2014).

72. Doig, C.J., *et al.* Increased intestinal permeability is associated with the development of multiple organ dysfunction syndrome in critically ill ICU patients. *American journal of respiratory and critical care medicine* **158**, 444-451 (1998).

73. Tripathi, A., *et al.* Identification of human zonulin, a physiological modulator of tight junctions, as prehaptoglobin-2. *Proceedings of the National Academy of Sciences of the United States of America* **106**, 16799-16804 (2009).

74. Fasano, A., *et al.* Zonulin, a newly discovered modulator of intestinal permeability, and its expression in coeliac disease. *Lancet* **355**, 1518-1519 (2000).

75. Sturgeon, C. & Fasano, A. Zonulin, a regulator of epithelial and endothelial barrier functions, and its involvement in chronic inflammatory diseases. *Tissue Barriers* **4**, e1251384 (2016).

76. Arrieta, M.C., Madsen, K., Doyle, J. & Meddings, J. Reducing small intestinal permeability attenuates colitis in the IL10 gene-deficient mouse. *Gut* **58**, 41-48 (2009).

77. Kelly, C.P.*, et al.* Larazotide acetate in patients with coeliac disease undergoing a gluten challenge: a randomised placebo-controlled study. *Alimentary pharmacology & therapeutics* **37**, 252-262 (2013).

78. Leffler, D.A.*, et al.* A randomized, double-blind study of larazotide acetate to prevent the activation of celiac disease during gluten challenge. *Am J Gastroenterol* **107**, 1554-1562 (2012).

79. Tajik, N.*, et al.* Targeting zonulin and intestinal epithelial barrier function to prevent onset of arthritis. *Nature communications* **11**, 1995 (2020).

80. Watts, T.*, et al.* Role of the intestinal tight junction modulator zonulin in the pathogenesis of type I diabetes in BB diabetic-prone rats. *Proceedings of the National Academy of Sciences of the United States of America* **102**, 2916-2921 (2005).

81. Leffler, D.A.*, et al.* Larazotide acetate for persistent symptoms of celiac disease despite a gluten-free diet: a randomized controlled trial. *Gastroenterology* **148**, 1311-1319 e1316 (2015).

82. Paterson, B.M., Lammers, K.M., Arrieta, M.C., Fasano, A. & Meddings, J.B. The safety, tolerance, pharmacokinetic and pharmacodynamic effects of single doses of AT-1001 in coeliac disease subjects: a proof of concept study. *Alimentary pharmacology & therapeutics* **26**, 757-766 (2007).

83. Marquez, L.*, et al.* Effects of haptoglobin polymorphisms and deficiency on susceptibility to inflammatory bowel disease and on severity of murine colitis. *Gut* **61**, 528-534 (2012).

84. Papp, M.*, et al.* Haptoglobin polymorphism: a novel genetic risk factor for celiac disease development and its clinical manifestations. *Clinical chemistry* **54**, 697-704 (2008).

85. Costacou, T., Ferrell, R.E. & Orchard, T.J. Haptoglobin genotype: a determinant of cardiovascular complication risk in type 1 diabetes. *Diabetes* **57**, 1702-1706 (2008).

86. Costacou, T. & Orchard, T.J. The Haptoglobin genotype predicts cardio-renal mortality in type 1 diabetes. *J Diabetes Complications* **30**, 221-226 (2016).

87. Langlois, M.R. & Delanghe, J.R. Biological and clinical significance of haptoglobin polymorphism in humans. *Clinical chemistry* **42**, 1589-1600 (1996).

88. Wan, C.*, et al.* Abnormal changes of plasma acute phase proteins in schizophrenia and the relation between schizophrenia and haptoglobin (Hp) gene. *Amino acids* **32**, 101-108 (2007).

89. Curis, E.*, et al.* Almost all about citrulline in mammals. *Amino acids* **29**, 177-205 (2005).

90. Peters, J.H.*, et al.* Assessment of small bowel function in critical illness: potential role of citrulline metabolism. *J Intensive Care Med* **26**, 105-110 (2011).

91. Kao, C.C.*, et al.* The Microbiome, Intestinal Function, and Arginine Metabolism of Healthy Indian Women Are Different from Those of American and Jamaican Women. *The Journal of nutrition* **146**, 706-713 (2015).

92. Batista, M.A.*, et al.* Pretreatment with citrulline improves gut barrier after intestinal obstruction in mice. *JPEN. Journal of parenteral and enteral nutrition* **36**, 69-76 (2012).

93. Okamoto, M., Hidaka, A., Toyama, M. & Baba, M. Galectin-3 is involved in HIV-1 expression through NF-kappaB activation and associated with Tat in latently infected cells. *Virus research* **260**, 86-93 (2019).

94. Wang, W.H.*, et al.* The role of galectins in virus infection - A systemic literature review. *J Microbiol Immunol Infect* (2019).

95. Colomb, F.*, et al.* Galectin-9 Mediates HIV Transcription by Inducing TCR-Dependent ERK Signaling. *Frontiers in immunology* **10**, 267 (2019).

96. Chen, Y.J.*, et al.* Galectin-3 Enhances Avian H5N1 Influenza A Virus-Induced Pulmonary Inflammation by Promoting NLRP3 Inflammasome Activation. *The American journal of pathology* **188**, 1031-1042 (2018).

97. Mackinnon, A.C.*, et al.* Regulation of transforming growth factor-beta1-driven lung fibrosis by galectin-3. *American journal of respiratory and critical care medicine* **185**, 537-546 (2012).

98. Caniglia, J.L., Guda, M.R., Asuthkar, S., Tsung, A.J. & Velpula, K.K. A potential role for Galectin-3 inhibitors in the treatment of COVID-19. *PeerJ* **8**, e9392 (2020).

99. Caniglia, J.L., Asuthkar, S., Tsung, A.J., Guda, M.R. & Velpula, K.K. Immunopathology of galectin-3: an increasingly promising target in COVID-19. *F1000Res* **9**, 1078 (2020).

100. Li, J., *et al.* The mitophagy effector FUNDC1 controls mitochondrial reprogramming and cellular plasticity in cancer cells. *Science signaling* **13**(2020).

101. Alicea, G.M., *et al.* Changes in Aged Fibroblast Lipid Metabolism Induce Age-Dependent Melanoma Cell Resistance to Targeted Therapy via the Fatty Acid Transporter FATP2. *Cancer Discov* **10**, 1282-1295 (2020).

102. Gonthier, M.P., *et al.* Microbial aromatic acid metabolites formed in the gut account for a major fraction of the polyphenols excreted in urine of rats fed red wine polyphenols. *The Journal of nutrition* **133**, 461-467 (2003).

103. Marhuenda-Munoz, M., *et al.* Microbial Phenolic Metabolites: Which Molecules Actually Have an Effect on Human Health? *Nutrients* **11**(2019).

104. Pellock, S.J. & Redinbo, M.R. Glucuronides in the gut: Sugar-driven symbioses between microbe and host. *The Journal of biological chemistry* **292**, 8569-8576 (2017).

105. Monagas, M., *et al.* Insights into the metabolism and microbial biotransformation of dietary flavan-3-ols and the bioactivity of their metabolites. *Food Funct* **1**, 233-253 (2010).

106. Zhitao, H., *et al. Research Square* (2020).

107. Coman, V. & Vodnar, D.C. Hydroxycinnamic acids and human health: recent advances. *J Sci Food Agric* **100**, 483-499 (2020).

108. Nicholson, J.K., *et al.* Host-Gut Microbiota Metabolic Interactions. *Science* **336**, 1262-1267 (2012).

109. Pallares-Méndez, R., Aguilar-Salinas, C.A., Cruz-Bautista, I. & del Bosque-Plata, L. Metabolomics in diabetes, a review. *Annals of Medicine* **48**, 89-102 (2016).

110. Skrzypecki, J., Nieweglowska, K. & Samborowska, E. Valeric Acid, a Gut Microbiota Product, Penetrates to the Eye and Lowers Intraocular Pressure in Rats. *Nutrients* **12**(2020).

111. Selkrig, J., Wong, P., Zhang, X. & Pettersson, S. Metabolic tinkering by the gut microbiome: Implications for brain development and function. *Gut Microbes* **5**, 369-380 (2014).

112. Farowski, F., *et al.* Assessment of urinary 3-indoxyl sulfate as a marker for gut microbiota diversity and abundance of Clostridiales. *Gut Microbes* **10**, 133-141 (2019).

113. Huang, Y.Y., Martinez-Del Campo, A. & Balskus, E.P. Anaerobic 4-hydroxyproline utilization: Discovery of a new glycyl radical enzyme in the human gut microbiome uncovers a widespread microbial metabolic activity. *Gut Microbes* **9**, 437-451 (2018).

114. Rea, K., Dinan, T.G. & Cryan, J.F. The microbiome: A key regulator of stress and neuroinflammation. *Neurobiol Stress* **4**, 23-33 (2016).

115. Pan, L.*, et al.* Abnormal metabolism of gut microbiota reveals the possible molecular mechanism of nephropathy induced by hyperuricemia. *Acta Pharm Sin B* **10**, 249-261 (2020).

116. Molinero, N., Ruiz, L., Sanchez, B., Margolles, A. & Delgado, S. Intestinal Bacteria Interplay With Bile and Cholesterol Metabolism: Implications on Host Physiology. *Front Physiol* **10**, 185 (2019).

117. Arias, N.*, et al.* The Relationship between Choline Bioavailability from Diet, Intestinal Microbiota Composition, and Its Modulation of Human Diseases. *Nutrients* **12**(2020).

118. Maekawa, M.*, et al.* Butyrate and propionate production from D-mannitol in the large intestine of pig and rat. *Microbial Ecology in Health and Disease* **17**, 169-176 (2005).

119. Jain, A., Li, X.H. & Chen, W.N. An untargeted fecal and urine metabolomics analysis of the interplay between the gut microbiome, diet and human metabolism in Indian and Chinese adults. *Scientific reports* **9**, 9191 (2019).

120. Utzschneider, K.M., Kratz, M., Damman, C.J. & Hullar, M. Mechanisms Linking the Gut Microbiome and Glucose Metabolism. *J Clin Endocrinol Metab* **101**, 1445-1454 (2016).

121. Mathewson, N.D.*, et al.* Gut microbiome-derived metabolites modulate intestinal epithelial cell damage and mitigate graft-versus-host disease. *Nat Immunol* **17**, 505-513 (2016).

122. Ridlon, J.M., Kang, D.J., Hylemon, P.B. & Bajaj, J.S. Bile acids and the gut microbiome. *Curr Opin Gastroenterol* **30**, 332-338 (2014).

123. Xu, M.*, et al.* Deoxycholic Acid-Induced Gut Dysbiosis Disrupts Bile Acid Enterohepatic Circulation and Promotes Intestinal Inflammation. *Dig Dis Sci* (2020).

124. Di Rienzi, S.C. & Britton, R.A. Adaptation of the Gut Microbiota to Modern Dietary Sugars and Sweeteners. *Adv Nutr* **11**, 616-629 (2020).

125. Craft, I.L., Geddes, D., Hyde, C.W., Wise, I.J. & Matthews, D.M. Absorption and malabsorption of glycine and glycine peptides in man. *Gut* **9**, 425-437 (1968).

126. Koistinen, V.M., *et al.* Contribution of gut microbiota to metabolism of dietary glycine betaine in mice and in vitro colonic fermentation. *Microbiome* **7**, 103 (2019).

127. Yasumoto, K. & Sugiyama, K. Perturbation by Bestatin of Glycyl-l-leucine Absorption in Isolated Epithelial Cells from Rat Intestine. *Agricultural and Biological Chemistry* **44**, 1339-1344 (1980).

128. Gao, J., *et al.* Impact of the Gut Microbiota on Intestinal Immunity Mediated by Tryptophan Metabolism. *Front Cell Infect Microbiol* **8**, 13 (2018).

129. Krautkramer, K.A., Fan, J. & Backhed, F. Gut microbial metabolites as multi-kingdom intermediates. *Nat Rev Microbiol* (2020).

130. Luo, L., *et al.* Association between metabolic profile and microbiomic changes in rats with functional dyspepsia. *RSC Advances* **8**, 20166-20181 (2018).

131. Zhang, L., *et al.* Metabolic phenotypes and the gut microbiota in response to dietary resistant starch type 2 in normal-weight subjects: a randomized crossover trial. *Scientific reports* **9**, 4736 (2019).

132. Oliphant, K. & Allen-Vercoe, E. Macronutrient metabolism by the human gut microbiome: major fermentation by-products and their impact on host health. *Microbiome* **7**, 91 (2019).

133. Kong, J.-Q. Phenylalanine ammonia-lyase, a key component used for phenylpropanoids production by metabolic engineering. *RSC Advances* **5**, 62587-62603 (2015).

134. Heianza, Y., *et al.* Long-Term Changes in Gut Microbial Metabolite Trimethylamine N-Oxide and Coronary Heart Disease Risk. *Journal of the American College of Cardiology* **75**, 763-772 (2020).

1. Guan, W.J., *et al.* Clinical Characteristics of Coronavirus Disease 2019 in China. *The New England journal of medicine* **382**, 1708-1720 (2020).

2. Gandhi, R.T., Lynch, J.B. & Del Rio, C. Mild or Moderate Covid-19. *The New England journal of medicine* (2020).

3. Grasselli, G., *et al.* Baseline Characteristics and Outcomes of 1591 Patients Infected With SARS-CoV-2 Admitted to ICUs of the Lombardy Region, Italy. *Jama* **323**, 1574-1581 (2020).

4. Richardson, S., *et al.* Presenting Characteristics, Comorbidities, and Outcomes Among 5700 Patients Hospitalized With COVID-19 in the New York City Area. *Jama* **323**, 2052-2059 (2020).

5. Chen, N., *et al.* Epidemiological and clinical characteristics of 99 cases of 2019 novel coronavirus pneumonia in Wuhan, China: a descriptive study. *Lancet* **395**, 507-513 (2020).

6. Blanco-Melo, D., *et al.* Imbalanced Host Response to SARS-CoV-2 Drives Development of COVID-19. *Cell* **181**, 1036-1045 e1039 (2020).

7. Chen, G., *et al.* Clinical and immunological features of severe and moderate coronavirus disease 2019. *The Journal of clinical investigation* **130**, 2620-2629 (2020).

8. Mehta, P., *et al.* COVID-19: consider cytokine storm syndromes and immunosuppression. *Lancet* **395**, 1033-1034 (2020).

9. Huang, C., *et al.* Clinical features of patients infected with 2019 novel coronavirus in Wuhan, China. *Lancet* **395**, 497-506 (2020).

10. Risitano, A.M., *et al.* Complement as a target in COVID-19? *Nature reviews. Immunology* (2020).

11. Dumas, A., Bernard, L., Poquet, Y., Lugo-Villarino, G. & Neyrolles, O. The role of the lung microbiota and the gut-lung axis in respiratory infectious diseases. *Cellular microbiology* **20**, e12966 (2018).

12. Frati, F., *et al.* The Role of the Microbiome in Asthma: The Gut(-)Lung Axis. *International journal of molecular sciences* **20**(2018).

13. Mukherjee, S. & Hanidziar, D. More of the Gut in the Lung: How Two Microbiomes Meet in ARDS. *Yale J Biol Med* **91**, 143-149 (2018).

14. Dickson, R.P., *et al.* Enrichment of the lung microbiome with gut bacteria in sepsis and the acute respiratory distress syndrome. *Nat Microbiol* **1**, 16113 (2016).

15. Lamers, M.M., *et al.* SARS-CoV-2 productively infects human gut enterocytes. *Science* (2020).

16. Brenchley, J.M., *et al.* CD4+ T cell depletion during all stages of HIV disease occurs predominantly in the gastrointestinal tract. *J. Exp. Med.* **200**, 749-759 (2004).

17. Niessen, C.M. Tight junctions/adherens junctions: basic structure and function. *The Journal of investigative dermatology* **127**, 2525-2532 (2007).

18. Turner, J.R. Intestinal mucosal barrier function in health and disease. *Nature reviews. Immunology* **9**, 799-809 (2009).

19. O'Toole, P.W. & Jeffery, I.B. Gut microbiota and aging. *Science* **350**, 1214-1215 (2015).

20. Thevaranjan, N., *et al.* Age-Associated Microbial Dysbiosis Promotes Intestinal Permeability, Systemic Inflammation, and Macrophage Dysfunction. *Cell host & microbe* **21**, 455-466 e454 (2017).

21. Kim, K.A., Jeong, J.J., Yoo, S.Y. & Kim, D.H. Gut microbiota lipopolysaccharide accelerates inflamm-aging in mice. *BMC microbiology* **16**, 9 (2016).

22. Fransen, F., *et al.* Aged Gut Microbiota Contributes to Systemical Inflammaging after Transfer to Germ-Free Mice. *Frontiers in immunology* **8**, 1385 (2017).

23. Zhang, C., *et al.* Structural modulation of gut microbiota in life-long calorie-restricted mice. *Nature communications* **4**, 2163 (2013).

24. Klingelhoefer, L. & Reichmann, H. Pathogenesis of Parkinson disease--the gut-brain axis and environmental factors. *Nat Rev Neurol* **11**, 625-636 (2015).

25. Fragkos, K.C. & Forbes, A. Citrulline as a marker of intestinal function and absorption in clinical settings: A systematic review and meta-analysis. *United European Gastroenterol J* **6**, 181-191 (2018).

26. Fujisaka, S., *et al.* Diet, Genetics, and the Gut Microbiome Drive Dynamic Changes in Plasma Metabolites. *Cell Rep* **22**, 3072-3086 (2018).

27. Kurilshikov, A., *et al.* Gut Microbial Associations to Plasma Metabolites Linked to Cardiovascular Phenotypes and Risk. *Circ Res* **124**, 1808-1820 (2019).

28. Mayneris-Perxachs, J. & Fernandez-Real, J.M. Exploration of the microbiota and metabolites within body fluids could pinpoint novel disease mechanisms. *FEBS J* **287**, 856-865 (2020).

29. Davaatseren, M., *et al.* Poly-gamma-glutamic acid attenuates angiogenesis and inflammation in experimental colitis. *Mediators Inflamm* **2013**, 982383 (2013).

30. Villeda-Gonzalez, J.D., *et al.* Nicotinamide reduces inflammation and oxidative stress via the cholinergic system in fructose-induced metabolic syndrome in rats. *Life Sci* **250**, 117585 (2020).

31. Karsten, C.M., *et al.* Anti-inflammatory activity of IgG1 mediated by Fc galactosylation and association of FcgammaRIIB and dectin-1. *Nature medicine* **18**, 1401-1406 (2012).

32. Cao, Y., Rocha, E.R. & Smith, C.J. Efficient utilization of complex N-linked glycans is a selective advantage for Bacteroides fragilis in extraintestinal infections. *Proceedings of the National Academy of Sciences of the United States of America* **111**, 12901-12906 (2014).

33. Simurina, M., *et al.* Glycosylation of Immunoglobulin G Associates With Clinical Features of Inflammatory Bowel Diseases. *Gastroenterology* **154**, 1320-1333 e1310 (2018).

34. Bamba, T., Matsuda, H., Endo, M. & Fujiyama, Y. The pathogenic role of Bacteroides vulgatus in patients with ulcerative colitis. *J Gastroenterol* **30 Suppl 8**, 45-47 (1995).

35. Huang, Y.L., Chassard, C., Hausmann, M., von Itzstein, M. & Hennet, T. Sialic acid catabolism drives intestinal inflammation and microbial dysbiosis in mice. *Nature communications* **6**, 8141 (2015).

36. Matsuda, H., *et al.* Characterization of antibody responses against rectal mucosa-associated bacterial flora in patients with ulcerative colitis. *J Gastroenterol Hepatol* **15**, 61-68 (2000).

37. Bloom, S.M., *et al.* Commensal Bacteroides species induce colitis in host-genotype-specific fashion in a mouse model of inflammatory bowel disease. *Cell host & microbe* **9**, 390-403 (2011).

38. Monaghan, T.M., *et al.* Decreased Complexity of Serum N-glycan Structures Associates with Successful Fecal Microbiota Transplantation for Recurrent Clostridioides difficile Infection. *Gastroenterology* **157**, 1676-1678 e1673 (2019).

39. Fasano, A. Zonulin and its regulation of intestinal barrier function: the biological door to inflammation, autoimmunity, and cancer. *Physiol Rev* **91**, 151-175 (2011).

40. El Asmar, R., *et al.* Host-dependent zonulin secretion causes the impairment of the small intestine barrier function after bacterial exposure. *Gastroenterology* **123**, 1607-1615 (2002).

41. Wood Heickman, L.K., DeBoer, M.D. & Fasano, A. Zonulin as a potential putative biomarker of risk for shared type 1 diabetes and celiac disease autoimmunity. *Diabetes Metab Res Rev* **36**, e3309 (2020).

42. Muta, T. & Takeshige, K. Essential roles of CD14 and lipopolysaccharide-binding protein for activation of toll-like receptor (TLR)2 as well as TLR4 Reconstitution of TLR2- and TLR4-activation by distinguishable ligands in LPS preparations. *Eur J Biochem* **268**, 4580-4589 (2001).

43. Morris, A., *et al.* Serum (1-->3)-beta-D-glucan levels in HIV-infected individuals are associated with immunosuppression, inflammation, and cardiopulmonary function. *Journal of acquired immune deficiency syndromes* **61**, 462-468 (2012).

44. Isnard, S., *et al.* Plasma Levels of C-Type Lectin REG3alpha and Gut Damage in People With Human Immunodeficiency Virus. *The Journal of infectious diseases* **221**, 110-121 (2020).

45. Whitt, D.D. & Demoss, R.D. Effect of microflora on the free amino acid distribution in various regions of the mouse gastrointestinal tract. *Appl Microbiol* **30**, 609-615 (1975).

46. Ma, N. & Ma, X. Dietary Amino Acids and the Gut-Microbiome-Immune Axis: Physiological Metabolism and Therapeutic Prospects. *Compr Rev Food Sci F* **18**, 221-242 (2019).

47. Blachier, F., Mariotti, F., Huneau, J.F. & Tome, D. Effects of amino acid-derived luminal metabolites on the colonic epithelium and physiopathological consequences. *Amino acids* **33**, 547-562 (2007).

48. Schaible, U.E. & Kaufmann, S.H. A nutritive view on the host-pathogen interplay. *Trends in microbiology* **13**, 373-380 (2005).

49. Mellor, A.L. & Munn, D.H. IDO expression by dendritic cells: tolerance and tryptophan catabolism. *Nature reviews. Immunology* **4**, 762-774 (2004).

50. Vujkovic-Cvijin, I., *et al.* Dysbiosis of the gut microbiota is associated with HIV disease progression and tryptophan catabolism. *Sci Transl Med* **5**, 193ra191 (2013).

51. Zhao, M., *et al.* Modulation of the Gut Microbiota during High-Dose Glycerol Monolaurate-Mediated Amelioration of Obesity in Mice Fed a High-Fat Diet. *mBio* **11**(2020).

52. Wahlstrom, A., Sayin, S.I., Marschall, H.U. & Backhed, F. Intestinal Crosstalk between Bile Acids and Microbiota and Its Impact on Host Metabolism. *Cell Metab* **24**, 41-50 (2016).

53. Liang, W., *et al.* Alterations Of Glycerophospholipid And Fatty Acyl Metabolism In Multiple Brain Regions Of Schizophrenia Microbiota Recipient Mice. *Neuropsychiatr Dis Treat* **15**, 3219-3229 (2019).

54. Ehehalt, R., *et al.* Phosphatidylcholine and lysophosphatidylcholine in intestinal mucus of ulcerative colitis patients. A quantitative approach by nanoElectrospray-tandem mass spectrometry. *Scand J Gastroenterol* **39**, 737-742 (2004).

55. Tateno, H., Kuno, A., Itakura, Y. & Hirabayashi, J. A versatile technology for cellular glycomics using lectin microarray. *Methods in enzymology* **478**, 181-195 (2010).

56. Mao, R., *et al.* Manifestations and prognosis of gastrointestinal and liver involvement in patients with COVID-19: a systematic review and meta-analysis. *Lancet Gastroenterol Hepatol* **5**, 667-678 (2020).

57. Pan, L., *et al.* Clinical Characteristics of COVID-19 Patients With Digestive Symptoms in Hubei, China: A Descriptive, Cross-Sectional, Multicenter Study. *Am J Gastroenterol* **115**, 766-773 (2020).

58. Livanos, A.E., *et al.* Gastrointestinal involvement attenuates COVID-19 severity and mortality. *medRxiv*, 2020.2009.2007.20187666 (2020).

59. Ngai, J.C., *et al.* The long-term impact of severe acute respiratory syndrome on pulmonary function, exercise capacity and health status. *Respirology* **15**, 543-550 (2010).

60. Wu, Q., *et al.* Altered Lipid Metabolism in Recovered SARS Patients Twelve Years after Infection. *Scientific reports* **7**, 9110 (2017).

61. Vyboh, K., Jenabian, M.A., Mehraj, V. & Routy, J.P. HIV and the gut microbiota, partners in crime: breaking the vicious cycle to unearth new therapeutic targets. *Journal of immunology research* **2015**, 614127 (2015).

62. Vazquez-Castellanos, J.F., *et al.* Altered metabolism of gut microbiota contributes to chronic immune activation in HIV-infected individuals. *Mucosal Immunol* **8**, 760-772 (2015).

63. Dinh, D.M., *et al.* Intestinal microbiota, microbial translocation, and systemic inflammation in chronic HIV infection. *J Infect Dis* **211**, 19-27 (2015).

64. Knoop, K.A., McDonald, K.G., Kulkarni, D.H. & Newberry, R.D. Antibiotics promote inflammation through the translocation of native commensal colonic bacteria. *Gut* **65**, 1100-1109 (2016).

65. Brindle, J.T., *et al.* Rapid and noninvasive diagnosis of the presence and severity of coronary heart disease using 1H-NMR-based metabonomics. *Nat Med* **8**, 1439-1444 (2002).

66. Oeckl, P. & Otto, M. A Review on MS-Based Blood Biomarkers for Alzheimer's Disease. *Neurol Ther* **8**, 113-127 (2019).

67. Hennig, R., *et al.* Towards personalized diagnostics via longitudinal study of the human plasma N-glycome. *Biochim Biophys Acta* **1860**, 1728-1738 (2016).

68. Keser, T., *et al.* Increased plasma N-glycome complexity is associated with higher risk of type 2 diabetes. *Diabetologia* **60**, 2352-2360 (2017).

69. Trbojevic Akmacic, I., *et al.* Inflammatory bowel disease associates with proinflammatory potential of the immunoglobulin G glycome. *Inflamm Bowel Dis* **21**, 1237-1247 (2015).

70. Vuckovic, F., *et al.* IgG Glycome in Colorectal Cancer. *Clinical cancer research : an official journal of the American Association for Cancer Research* **22**, 3078-3086 (2016).

71. Akinkuolie, A.O., Buring, J.E., Ridker, P.M. & Mora, S. A novel protein glycan biomarker and future cardiovascular disease events. *Journal of the American Heart Association* **3**, e001221 (2014).

72. Doig, C.J., *et al.* Increased intestinal permeability is associated with the development of multiple organ dysfunction syndrome in critically ill ICU patients. *American journal of respiratory and critical care medicine* **158**, 444-451 (1998).

73. Tripathi, A., *et al.* Identification of human zonulin, a physiological modulator of tight junctions, as prehaptoglobin-2. *Proceedings of the National Academy of Sciences of the United States of America* **106**, 16799-16804 (2009).

74. Fasano, A., *et al.* Zonulin, a newly discovered modulator of intestinal permeability, and its expression in coeliac disease. *Lancet* **355**, 1518-1519 (2000).

75. Sturgeon, C. & Fasano, A. Zonulin, a regulator of epithelial and endothelial barrier functions, and its involvement in chronic inflammatory diseases. *Tissue Barriers* **4**, e1251384 (2016).

76. Arrieta, M.C., Madsen, K., Doyle, J. & Meddings, J. Reducing small intestinal permeability attenuates colitis in the IL10 gene-deficient mouse. *Gut* **58**, 41-48 (2009).

77. Kelly, C.P., *et al.* Larazotide acetate in patients with coeliac disease undergoing a gluten challenge: a randomised placebo-controlled study. *Alimentary pharmacology & therapeutics* **37**, 252-262 (2013).

78. Leffler, D.A., *et al.* A randomized, double-blind study of larazotide acetate to prevent the activation of celiac disease during gluten challenge. *Am J Gastroenterol* **107**, 1554-1562 (2012).

79. Tajik, N., *et al.* Targeting zonulin and intestinal epithelial barrier function to prevent onset of arthritis. *Nature communications* **11**, 1995 (2020).

80. Watts, T., *et al.* Role of the intestinal tight junction modulator zonulin in the pathogenesis of type I diabetes in BB diabetic-prone rats. *Proceedings of the National Academy of Sciences of the United States of America* **102**, 2916-2921 (2005).

81. Leffler, D.A., *et al.* Larazotide acetate for persistent symptoms of celiac disease despite a gluten-free diet: a randomized controlled trial. *Gastroenterology* **148**, 1311-1319 e1316 (2015).

82. Paterson, B.M., Lammers, K.M., Arrieta, M.C., Fasano, A. & Meddings, J.B. The safety, tolerance, pharmacokinetic and pharmacodynamic effects of single doses of AT-1001 in

coeliac disease subjects: a proof of concept study. *Alimentary pharmacology & therapeutics* **26**, 757-766 (2007).

83. Marquez, L.*, et al.* Effects of haptoglobin polymorphisms and deficiency on susceptibility to inflammatory bowel disease and on severity of murine colitis. *Gut* **61**, 528-534 (2012).

84. Papp, M.*, et al.* Haptoglobin polymorphism: a novel genetic risk factor for celiac disease development and its clinical manifestations. *Clinical chemistry* **54**, 697-704 (2008).

85. Costacou, T., Ferrell, R.E. & Orchard, T.J. Haptoglobin genotype: a determinant of cardiovascular complication risk in type 1 diabetes. *Diabetes* **57**, 1702-1706 (2008).

86. Costacou, T. & Orchard, T.J. The Haptoglobin genotype predicts cardio-renal mortality in type 1 diabetes. *J Diabetes Complications* **30**, 221-226 (2016).

87. Langlois, M.R. & Delanghe, J.R. Biological and clinical significance of haptoglobin polymorphism in humans. *Clinical chemistry* **42**, 1589-1600 (1996).

88. Wan, C.*, et al.* Abnormal changes of plasma acute phase proteins in schizophrenia and the relation between schizophrenia and haptoglobin (Hp) gene. *Amino acids* **32**, 101-108 (2007).

89. Curis, E.*, et al.* Almost all about citrulline in mammals. *Amino acids* **29**, 177-205 (2005).

90. Peters, J.H.*, et al.* Assessment of small bowel function in critical illness: potential role of citrulline metabolism. *J Intensive Care Med* **26**, 105-110 (2011).

91. Kao, C.C.*, et al.* The Microbiome, Intestinal Function, and Arginine Metabolism of Healthy Indian Women Are Different from Those of American and Jamaican Women. *The Journal of nutrition* **146**, 706-713 (2015).

92. Batista, M.A.*, et al.* Pretreatment with citrulline improves gut barrier after intestinal obstruction in mice. *JPEN. Journal of parenteral and enteral nutrition* **36**, 69-76 (2012).

93. Okamoto, M., Hidaka, A., Toyama, M. & Baba, M. Galectin-3 is involved in HIV-1 expression through NF-kappaB activation and associated with Tat in latently infected cells. *Virus research* **260**, 86-93 (2019).

94. Wang, W.H.*, et al.* The role of galectins in virus infection - A systemic literature review. *J Microbiol Immunol Infect* (2019).

95. Colomb, F.*, et al.* Galectin-9 Mediates HIV Transcription by Inducing TCR-Dependent ERK Signaling. *Frontiers in immunology* **10**, 267 (2019).

96. Chen, Y.J.*, et al.* Galectin-3 Enhances Avian H5N1 Influenza A Virus-Induced Pulmonary Inflammation by Promoting NLRP3 Inflammasome Activation. *The American journal of pathology* **188**, 1031-1042 (2018).

97. Mackinnon, A.C., *et al.* Regulation of transforming growth factor-beta1-driven lung fibrosis by galectin-3. *American journal of respiratory and critical care medicine* **185**, 537-546 (2012).

98. Caniglia, J.L., Guda, M.R., Asuthkar, S., Tsung, A.J. & Velpula, K.K. A potential role for Galectin-3 inhibitors in the treatment of COVID-19. *PeerJ* **8**, e9392 (2020).

99. Caniglia, J.L., Asuthkar, S., Tsung, A.J., Guda, M.R. & Velpula, K.K. Immunopathology of galectin-3: an increasingly promising target in COVID-19. *F1000Res* **9**, 1078 (2020).

100. Li, J., *et al.* The mitophagy effector FUNDC1 controls mitochondrial reprogramming and cellular plasticity in cancer cells. *Science signaling* **13**(2020).

101. Alicea, G.M., *et al.* Changes in Aged Fibroblast Lipid Metabolism Induce Age-Dependent Melanoma Cell Resistance to Targeted Therapy via the Fatty Acid Transporter FATP2. *Cancer Discov* **10**, 1282-1295 (2020).

102. Gonthier, M.P., *et al.* Microbial aromatic acid metabolites formed in the gut account for a major fraction of the polyphenols excreted in urine of rats fed red wine polyphenols. *The Journal of nutrition* **133**, 461-467 (2003).

103. Marhuenda-Munoz, M., *et al.* Microbial Phenolic Metabolites: Which Molecules Actually Have an Effect on Human Health? *Nutrients* **11**(2019).

104. Pellock, S.J. & Redinbo, M.R. Glucuronides in the gut: Sugar-driven symbioses between microbe and host. *The Journal of biological chemistry* **292**, 8569-8576 (2017).

105. Monagas, M., *et al.* Insights into the metabolism and microbial biotransformation of dietary flavan-3-ols and the bioactivity of their metabolites. *Food Funct* **1**, 233-253 (2010).

106. Zhitao, H., *et al. Research Square* (2020).

107. Coman, V. & Vodnar, D.C. Hydroxycinnamic acids and human health: recent advances. *J Sci Food Agric* **100**, 483-499 (2020).

108. Nicholson, J.K., *et al.* Host-Gut Microbiota Metabolic Interactions. *Science* **336**, 1262-1267 (2012).

109. Pallares-Méndez, R., Aguilar-Salinas, C.A., Cruz-Bautista, I. & del Bosque-Plata, L. Metabolomics in diabetes, a review. *Annals of Medicine* **48**, 89-102 (2016).

110. Skrzypecki, J., Nieweglowska, K. & Samborowska, E. Valeric Acid, a Gut Microbiota Product, Penetrates to the Eye and Lowers Intraocular Pressure in Rats. *Nutrients* **12**(2020).

111. Selkrig, J., Wong, P., Zhang, X. & Pettersson, S. Metabolic tinkering by the gut microbiome: Implications for brain development and function. *Gut Microbes* **5**, 369-380 (2014).

112. Farowski, F., *et al.* Assessment of urinary 3-indoxyl sulfate as a marker for gut microbiota diversity and abundance of Clostridiales. *Gut Microbes* **10**, 133-141 (2019).

113. Huang, Y.Y., Martinez-Del Campo, A. & Balskus, E.P. Anaerobic 4-hydroxyproline utilization: Discovery of a new glycyl radical enzyme in the human gut microbiome uncovers a widespread microbial metabolic activity. *Gut Microbes* **9**, 437-451 (2018).

114. Rea, K., Dinan, T.G. & Cryan, J.F. The microbiome: A key regulator of stress and neuroinflammation. *Neurobiol Stress* **4**, 23-33 (2016).

115. Pan, L., *et al.* Abnormal metabolism of gut microbiota reveals the possible molecular mechanism of nephropathy induced by hyperuricemia. *Acta Pharm Sin B* **10**, 249-261 (2020).

116. Molinero, N., Ruiz, L., Sanchez, B., Margolles, A. & Delgado, S. Intestinal Bacteria Interplay With Bile and Cholesterol Metabolism: Implications on Host Physiology. *Front Physiol* **10**, 185 (2019).

117. Arias, N., *et al.* The Relationship between Choline Bioavailability from Diet, Intestinal Microbiota Composition, and Its Modulation of Human Diseases. *Nutrients* **12**(2020).

118. Maekawa, M., *et al.* Butyrate and propionate production from D-mannitol in the large intestine of pig and rat. *Microbial Ecology in Health and Disease* **17**, 169-176 (2005).

119. Jain, A., Li, X.H. & Chen, W.N. An untargeted fecal and urine metabolomics analysis of the interplay between the gut microbiome, diet and human metabolism in Indian and Chinese adults. *Scientific reports* **9**, 9191 (2019).

120. Utzschneider, K.M., Kratz, M., Damman, C.J. & Hullar, M. Mechanisms Linking the Gut Microbiome and Glucose Metabolism. *J Clin Endocrinol Metab* **101**, 1445-1454 (2016).

121. Mathewson, N.D., *et al.* Gut microbiome-derived metabolites modulate intestinal epithelial cell damage and mitigate graft-versus-host disease. *Nat Immunol* **17**, 505-513 (2016).

122. Ridlon, J.M., Kang, D.J., Hylemon, P.B. & Bajaj, J.S. Bile acids and the gut microbiome. *Curr Opin Gastroenterol* **30**, 332-338 (2014).

123. Xu, M., *et al.* Deoxycholic Acid-Induced Gut Dysbiosis Disrupts Bile Acid Enterohepatic Circulation and Promotes Intestinal Inflammation. *Dig Dis Sci* (2020).

124. Di Rienzi, S.C. & Britton, R.A. Adaptation of the Gut Microbiota to Modern Dietary Sugars and Sweeteners. *Adv Nutr* **11**, 616-629 (2020).

125. Craft, I.L., Geddes, D., Hyde, C.W., Wise, I.J. & Matthews, D.M. Absorption and malabsorption of glycine and glycine peptides in man. *Gut* **9**, 425-437 (1968).

126. Koistinen, V.M., *et al.* Contribution of gut microbiota to metabolism of dietary glycine betaine in mice and in vitro colonic fermentation. *Microbiome* **7**, 103 (2019).

127. Yasumoto, K. & Sugiyama, K. Perturbation by Bestatin of Glycyl-l-leucine Absorption in Isolated Epithelial Cells from Rat Intestine. *Agricultural and Biological Chemistry* **44**, 1339-1344 (1980).

128. Gao, J., *et al.* Impact of the Gut Microbiota on Intestinal Immunity Mediated by Tryptophan Metabolism. *Front Cell Infect Microbiol* **8**, 13 (2018).

129. Krautkramer, K.A., Fan, J. & Backhed, F. Gut microbial metabolites as multi-kingdom intermediates. *Nat Rev Microbiol* (2020).

130. Luo, L., *et al.* Association between metabolic profile and microbiomic changes in rats with functional dyspepsia. *RSC Advances* **8**, 20166-20181 (2018).

131. Zhang, L., *et al.* Metabolic phenotypes and the gut microbiota in response to dietary resistant starch type 2 in normal-weight subjects: a randomized crossover trial. *Scientific reports* **9**, 4736 (2019).

132. Oliphant, K. & Allen-Vercoe, E. Macronutrient metabolism by the human gut microbiome: major fermentation by-products and their impact on host health. *Microbiome* **7**, 91 (2019).

133. Kong, J.-Q. Phenylalanine ammonia-lyase, a key component used for phenylpropanoids production by metabolic engineering. *RSC Advances* **5**, 62587-62603 (2015).

134. Heianza, Y., *et al.* Long-Term Changes in Gut Microbial Metabolite Trimethylamine N-Oxide and Coronary Heart Disease Risk. *Journal of the American College of Cardiology* **75**, 763-772 (2020).

Figure 1

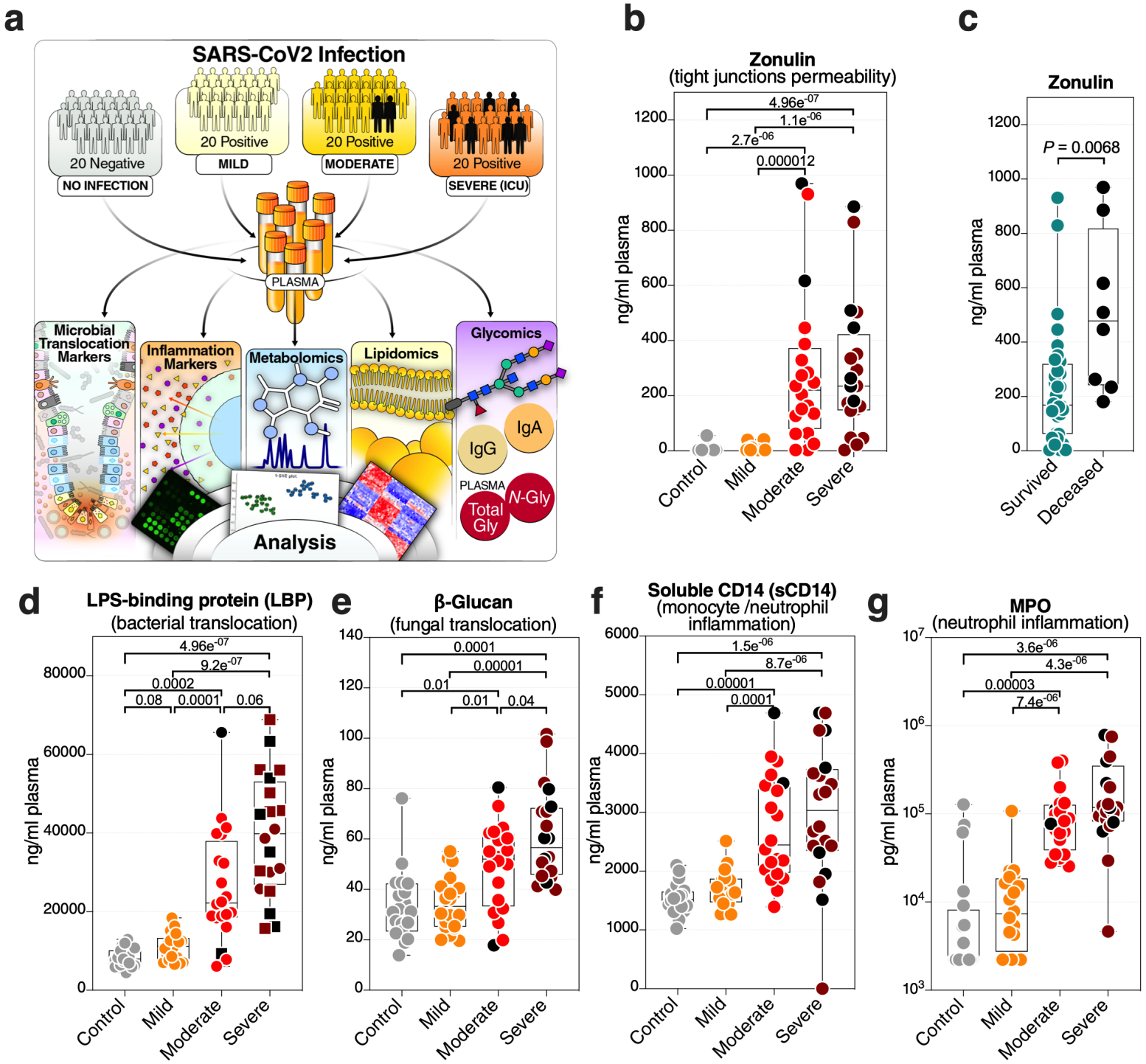
a
SARS-CoV2 Infection
20 Negative
NO INFECTION
20 Positive
MILD
20 Positive
MODERATE
20 Positive
SEVERE (ICU)
PLASMA
Microbial Translocation Markers
Inflammation Markers
Metabolomics
Lipidomics
Glycomics
IgA
IgG
PLASMA
Total Gly
N-Gly
Analysis
b
Zonulin
(tight junctions permeability)
ng/ml plasma
4.96e-07
1.1e-06
2.7e-06
0.000012
Control
Mild
Moderate
Severe
c
Zonulin
P = 0.0068
ng/ml plasma
Survived
Deceased
d
LPS-binding protein (LBP)
(bacterial translocation)
ng/ml plasma
4.96e-07
9.2e-07
0.0002
0.08
0.0001
0.06
Control
Mild
Moderate
Severe
e
β-Glucan
(fungal translocation)
ng/ml plasma
0.0001
0.00001
0.01
0.01
0.04
Control
Mild
Moderate
Severe
f
Soluble CD14 (sCD14)
(monocyte /neutrophil inflammation)
ng/ml plasma
1.5e-06
8.7e-06
0.00001
0.0001
Control
Mild
Moderate
Severe
g
MPO
(neutrophil inflammation)
pg/ml plasma
3.6e-06
4.3e-06
0.00003
7.4e-06
Control
Mild
Moderate
Severe

Figure 2

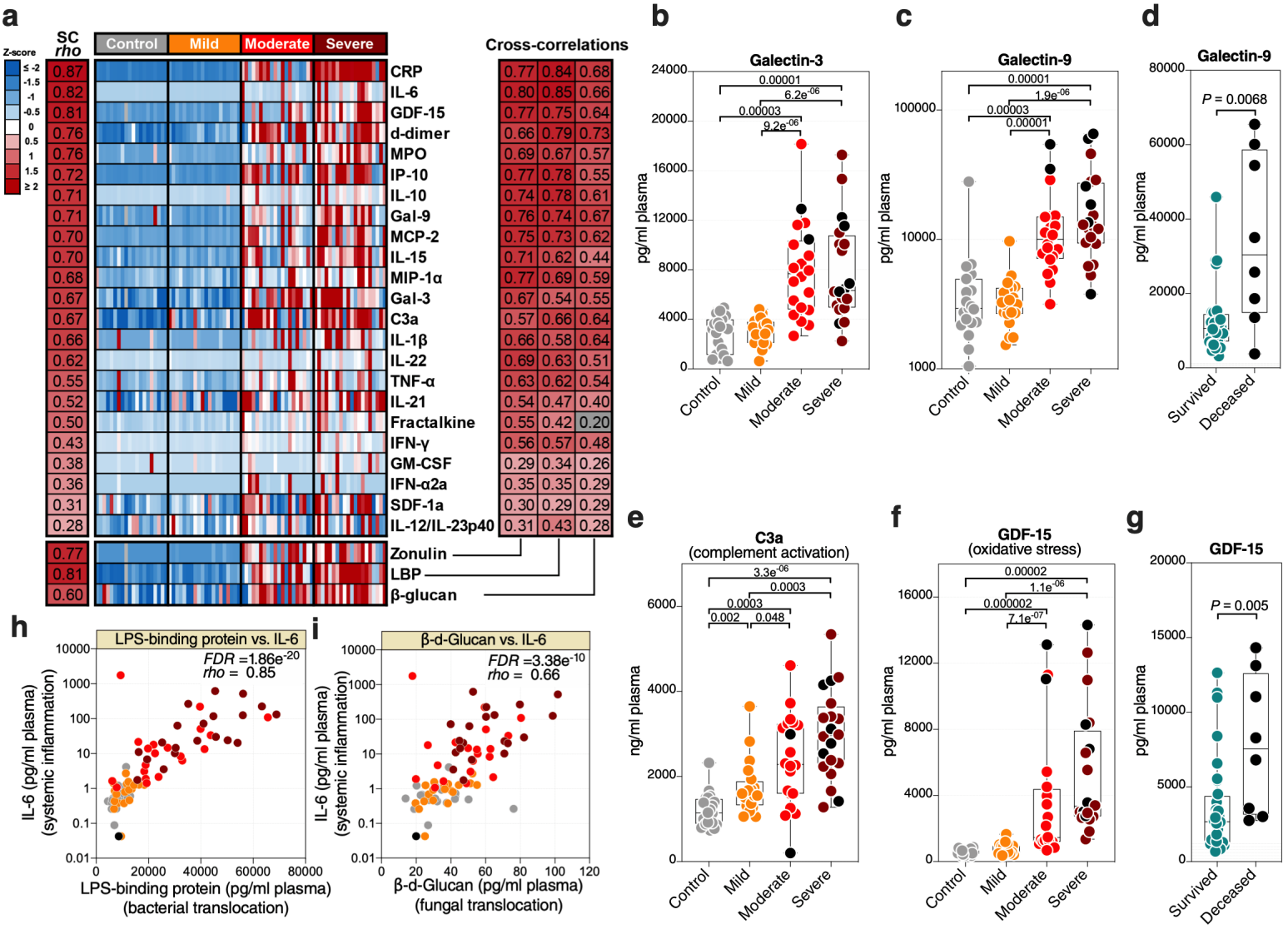
a
Z-score
SC rho
Control
Mild
Moderate
Severe
Cross-correlations
CRP
IL-6
GDF-15
d-dimer
MPO
IP-10
IL-10
Gal-9
MCP-2
IL-15
MIP-1α
Gal-3
C3a
IL-1β
IL-22
TNF-α
IL-21
Fractalkine
IFN-γ
GM-CSF
IFN-α2a
SDF-1a
IL-12/IL-23p40
Zonulin
LBP
β-glucan
b
Galectin-3
pg/ml plasma
Control
Mild
Moderate
Severe
c
Galectin-9
d
Galectin-9
P = 0.0068
Survived
Deceased
e
C3a
(complement activation)
ng/ml plasma
f
GDF-15
(oxidative stress)
g
GDF-15
P = 0.005
h
LPS-binding protein vs. IL-6
FDR =1.86e-20
rho = 0.85
IL-6 (pg/ml plasma)
(systemic inflammation)
LPS-binding protein (pg/ml plasma)
(bacterial translocation)
i
β-d-Glucan vs. IL-6
FDR =3.38e-10
rho = 0.66
β-d-Glucan (pg/ml plasma)
(fungal translocation)

Figure 3

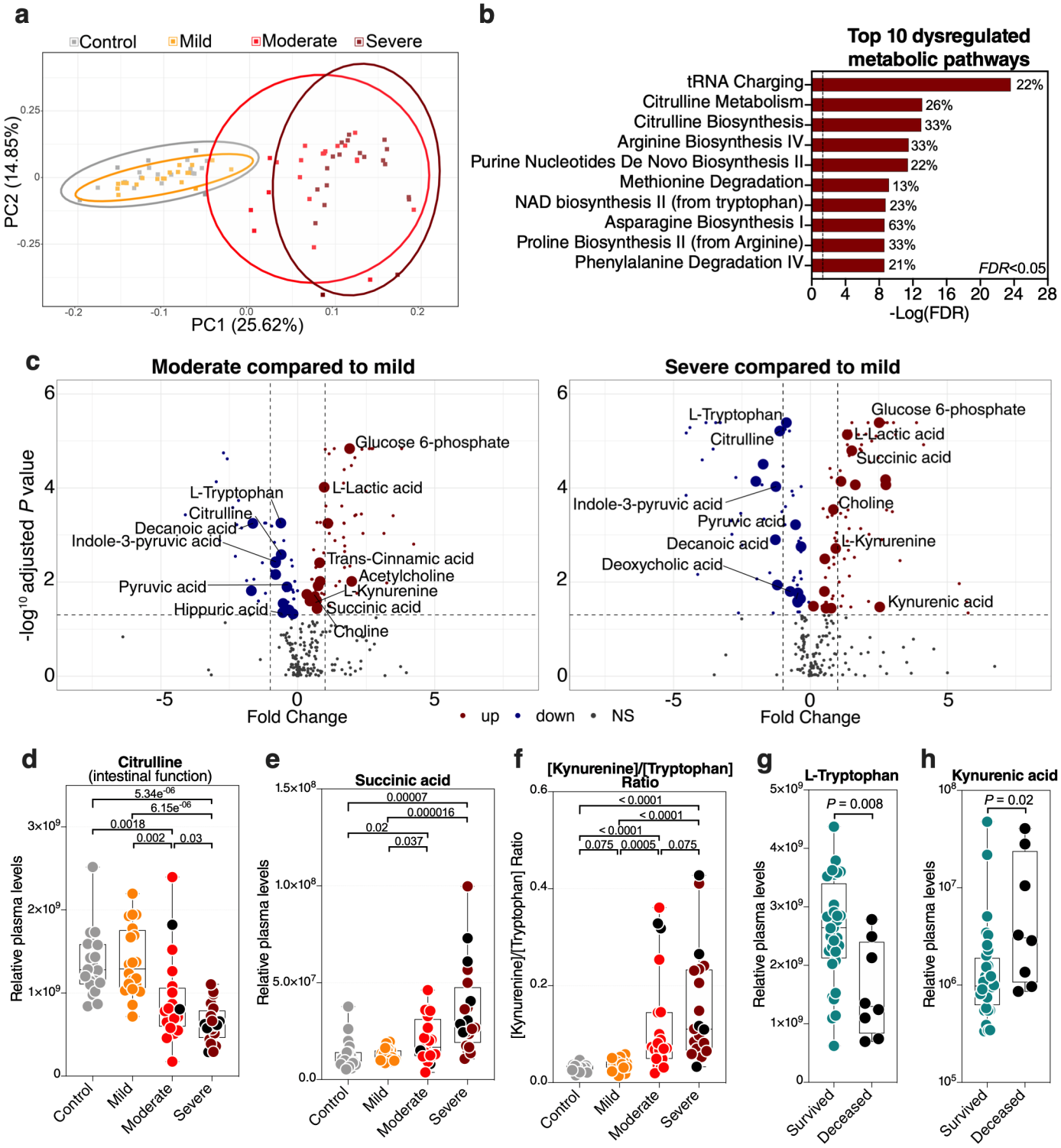
a
Control
Mild
Moderate
Severe
PC2 (14.85%)
PC1 (25.62%)
b
Top 10 dysregulated metabolic pathways
tRNA Charging
Citrulline Metabolism
Citrulline Biosynthesis
Arginine Biosynthesis IV
Purine Nucleotides De Novo Biosynthesis II
Methionine Degradation
NAD biosynthesis II (from tryptophan)
Asparagine Biosynthesis I
Proline Biosynthesis II (from Arginine)
Phenylalanine Degradation IV
22%
26%
33%
33%
22%
13%
23%
63%
33%
21%
FDR<0.05
-Log(FDR)
c
Moderate compared to mild
Severe compared to mild
-log10 adjusted P value
Fold Change
Glucose 6-phosphate
L-Lactic acid
L-Tryptophan
Citrulline
Decanoic acid
Indole-3-pyruvic acid
Trans-Cinnamic acid
Acetylcholine
Pyruvic acid
L-Kynurenine
Hippuric acid
Succinic acid
Choline
Deoxycholic acid
Kynurenic acid
up
down
NS
d
Citrulline (intestinal function)
Relative plasma levels
Control
Mild
Moderate
Severe
e
Succinic acid
f
[Kynurenine]/[Tryptophan] Ratio
g
L-Tryptophan
P = 0.008
Survived
Deceased
h
Kynurenic acid
P = 0.02

Figure 4

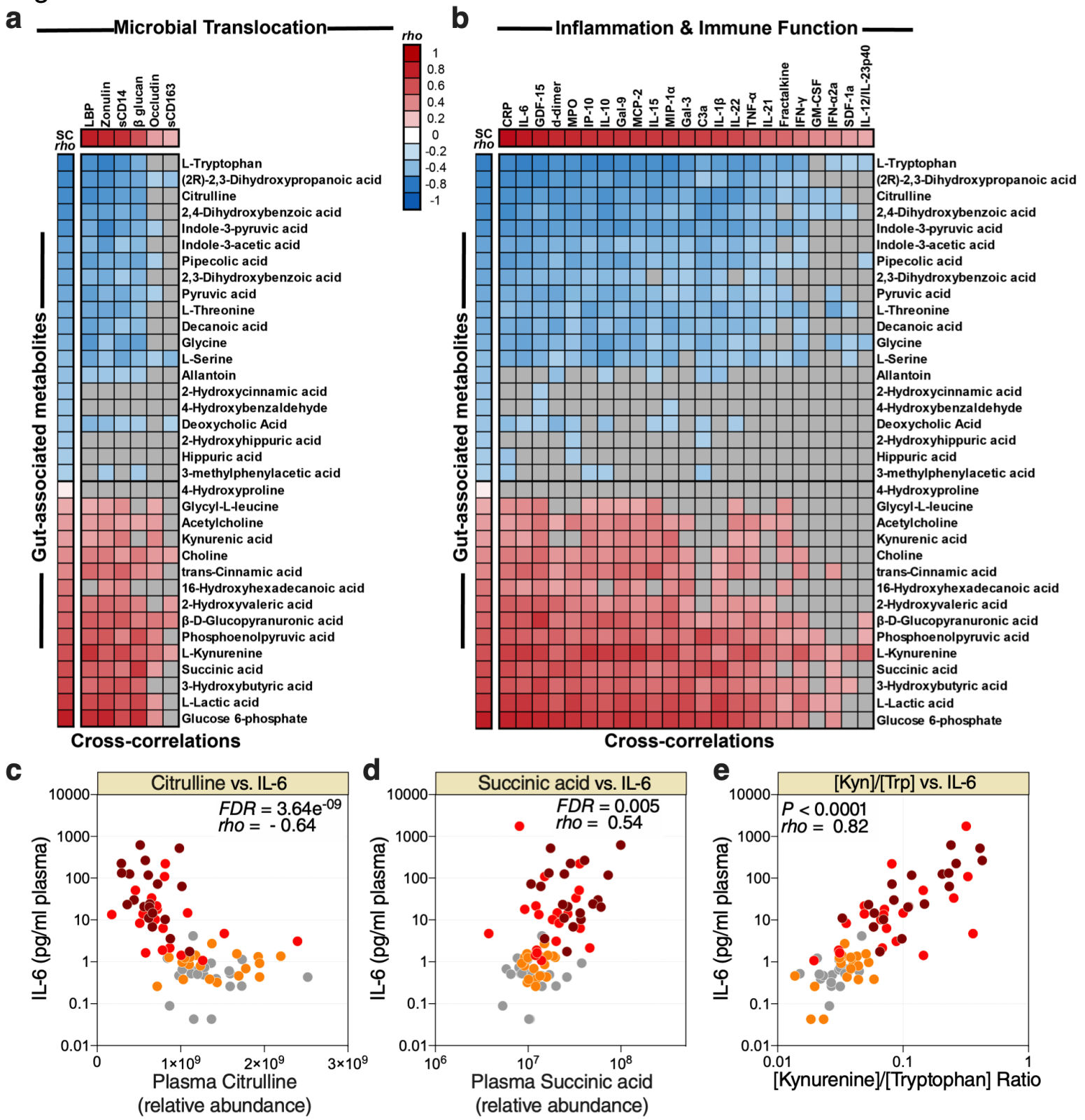
a
Microbial Translocation
rho
1
0.8
0.6
0.4
0.2
0
-0.2
-0.4
-0.8
-1
LBP
Zonulin
sCD14
β glucan
Occludin
sCD163
SC
rho
Gut-associated metabolites
L-Tryptophan
(2R)-2,3-Dihydroxypropanoic acid
Citrulline
2,4-Dihydroxybenzoic acid
Indole-3-pyruvic acid
Indole-3-acetic acid
Pipecolic acid
2,3-Dihydroxybenzoic acid
Pyruvic acid
L-Threonine
Decanoic acid
Glycine
L-Serine
Allantoin
2-Hydroxycinnamic acid
4-Hydroxybenzaldehyde
Deoxycholic Acid
2-Hydroxyhippuric acid
Hippuric acid
3-methylphenylacetic acid
4-Hydroxyproline
Glycyl-L-leucine
Acetylcholine
Kynurenic acid
Choline
trans-Cinnamic acid
16-Hydroxyhexadecanoic acid
2-Hydroxyvaleric acid
β-D-Glucopyranuronic acid
Phosphoenolpyruvic acid
L-Kynurenine
Succinic acid
3-Hydroxybutyric acid
L-Lactic acid
Glucose 6-phosphate
Cross-correlations
b
Inflammation & Immune Function
CRP
IL-6
GDF-15
d-dimer
MPO
IP-10
IL-10
Gal-9
MCP-2
IL-15
MIP-1α
Gal-3
C3a
IL-1β
IL-22
TNF-α
IL-21
Fractalkine
IFN-γ
GM-CSF
IFN-α2a
SDF-1a
IL-12/IL-23p40
SC
rho
Gut-associated metabolites
Cross-correlations
c
Citrulline vs. IL-6
FDR = 3.64e-09
rho = - 0.64
IL-6 (pg/ml plasma)
Plasma Citrulline
(relative abundance)
d
Succinic acid vs. IL-6
FDR = 0.005
rho = 0.54
IL-6 (pg/ml plasma)
Plasma Succinic acid
(relative abundance)
e
[Kyn]/[Trp] vs. IL-6
P < 0.0001
rho = 0.82
IL-6 (pg/ml plasma)
[Kynurenine]/[Tryptophan] Ratio

Figure 5

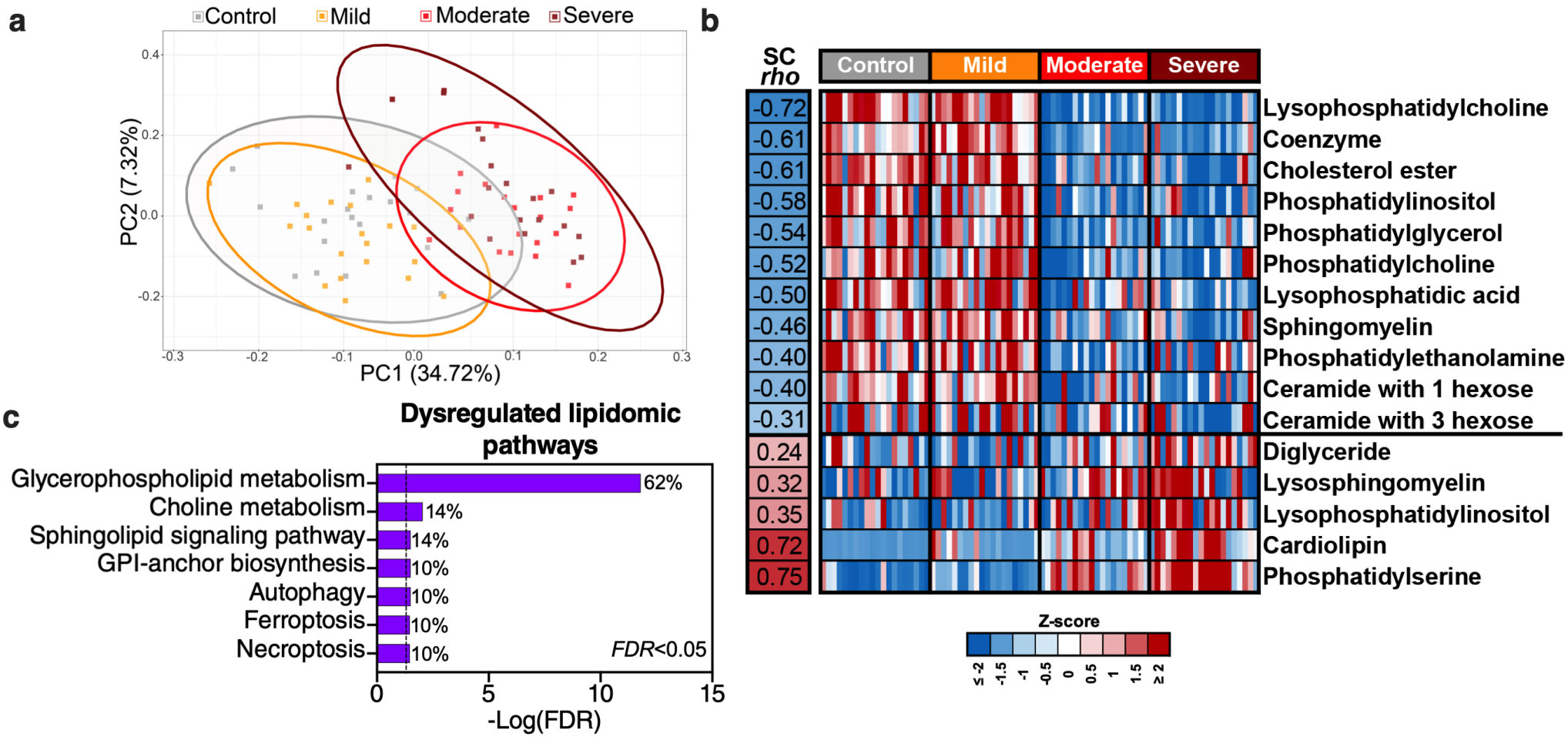
a
Control
Mild
Moderate
Severe
PC2 (7.32%)
PC1 (34.72%)
b
SC rho
Control
Mild
Moderate
Severe
-0.72 Lysophosphatidylcholine
-0.61 Coenzyme
-0.61 Cholesterol ester
-0.58 Phosphatidylinositol
-0.54 Phosphatidylglycerol
-0.52 Phosphatidylcholine
-0.50 Lysophosphatidic acid
-0.46 Sphingomyelin
-0.40 Phosphatidylethanolamine
-0.40 Ceramide with 1 hexose
-0.31 Ceramide with 3 hexose
0.24 Diglyceride
0.32 Lysosphingomyelin
0.35 Lysophosphatidylinositol
0.72 Cardiolipin
0.75 Phosphatidylserine
Z-score
c
Dysregulated lipidomic pathways
Glycerophospholipid metabolism 62%
Choline metabolism 14%
Sphingolipid signaling pathway 14%
GPI-anchor biosynthesis 10%
Autophagy 10%
Ferroptosis 10%
Necroptosis 10%
FDR<0.05
-Log(FDR)

Figure 6

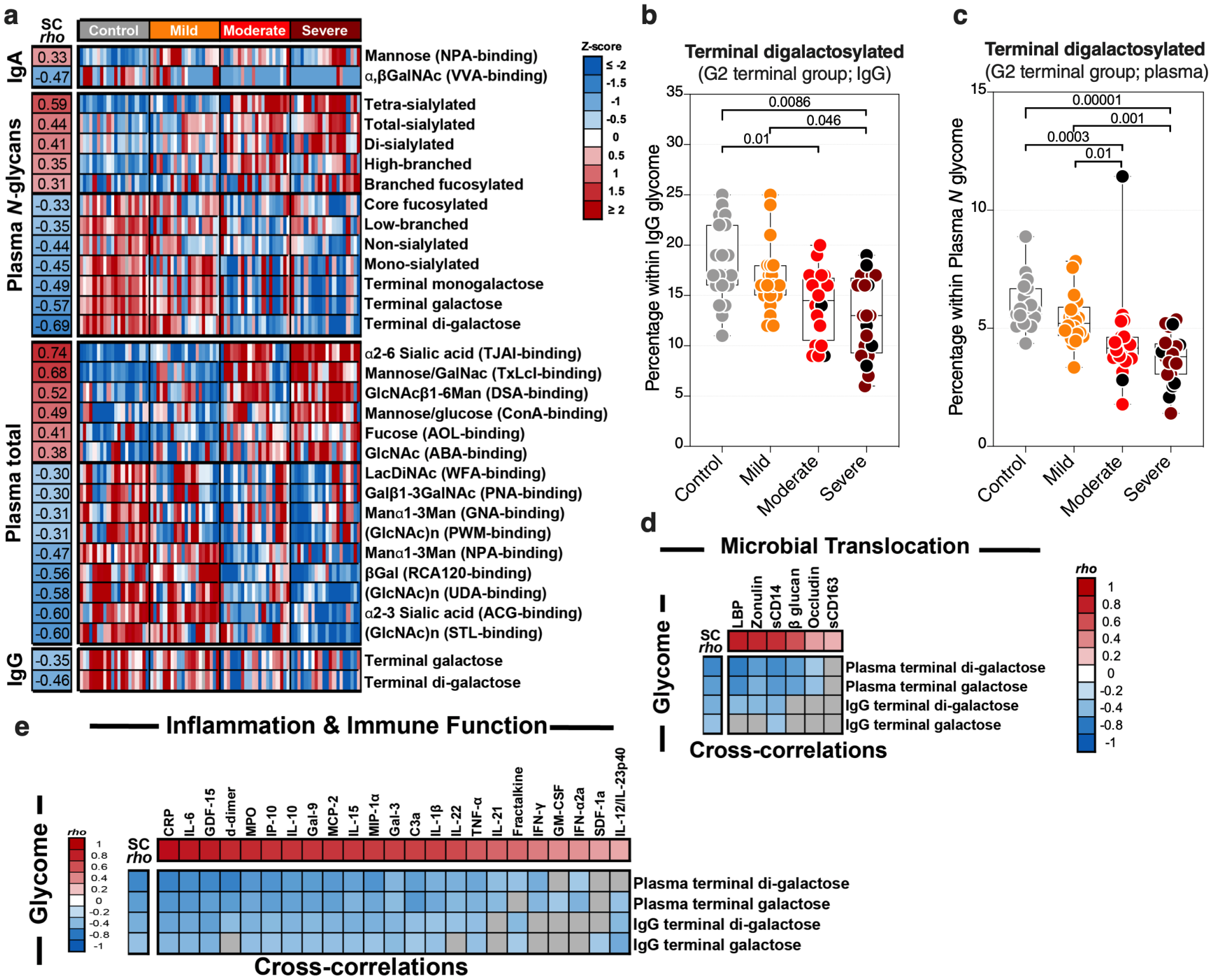
a
SC rho
Control
Mild
Moderate
Severe
IgA
0.33 Mannose (NPA-binding)
-0.47 α,βGalNAc (VVA-binding)
Plasma N-glycans
0.59 Tetra-sialylated
0.44 Total-sialylated
0.41 Di-sialylated
0.35 High-branched
0.31 Branched fucosylated
-0.33 Core fucosylated
-0.35 Low-branched
-0.44 Non-sialylated
-0.45 Mono-sialylated
-0.49 Terminal monogalactose
-0.57 Terminal galactose
-0.69 Terminal di-galactose
Plasma total
0.74 α2-6 Sialic acid (TJAI-binding)
0.68 Mannose/GalNac (TxLcI-binding)
0.52 GlcNAcβ1-6Man (DSA-binding)
0.49 Mannose/glucose (ConA-binding)
0.41 Fucose (AOL-binding)
0.38 GlcNAc (ABA-binding)
-0.30 LacDiNAc (WFA-binding)
-0.30 Galβ1-3GalNAc (PNA-binding)
-0.31 Manα1-3Man (GNA-binding)
-0.31 (GlcNAc)n (PWM-binding)
-0.47 Manα1-3Man (NPA-binding)
-0.56 βGal (RCA120-binding)
-0.58 (GlcNAc)n (UDA-binding)
-0.60 α2-3 Sialic acid (ACG-binding)
-0.60 (GlcNAc)n (STL-binding)
IgG
-0.35 Terminal galactose
-0.46 Terminal di-galactose
Z-score
≤ -2
-1.5
-1
-0.5
0
0.5
1
1.5
≥ 2
b
Terminal digalactosylated
(G2 terminal group; IgG)
Percentage within IgG glycome
0.0086
0.046
0.01
Control
Mild
Moderate
Severe
c
Terminal digalactosylated
(G2 terminal group; plasma)
Percentage within Plasma N glycome
0.00001
0.001
0.0003
0.01
Control
Mild
Moderate
Severe
d
Microbial Translocation
Glycome
SC rho
LBP
Zonulin
sCD14
β glucan
Occludin
sCD163
Plasma terminal di-galactose
Plasma terminal galactose
IgG terminal di-galactose
IgG terminal galactose
Cross-correlations
rho
1
0.8
0.6
0.4
0.2
0
-0.2
-0.4
-0.8
-1
e
Inflammation & Immune Function
Glycome
rho
SC rho
CRP
IL-6
GDF-15
d-dimer
MPO
IP-10
IL-10
Gal-9
MCP-2
IL-15
MIP-1α
Gal-3
C3a
IL-1β
IL-22
TNF-α
IL-21
Fractalkine
IFN-γ
GM-CSF
IFN-α2a
SDF-1a
IL-12/IL-23p40
Plasma terminal di-galactose
Plasma terminal galactose
IgG terminal di-galactose
IgG terminal galactose
Cross-correlations

Figure 7

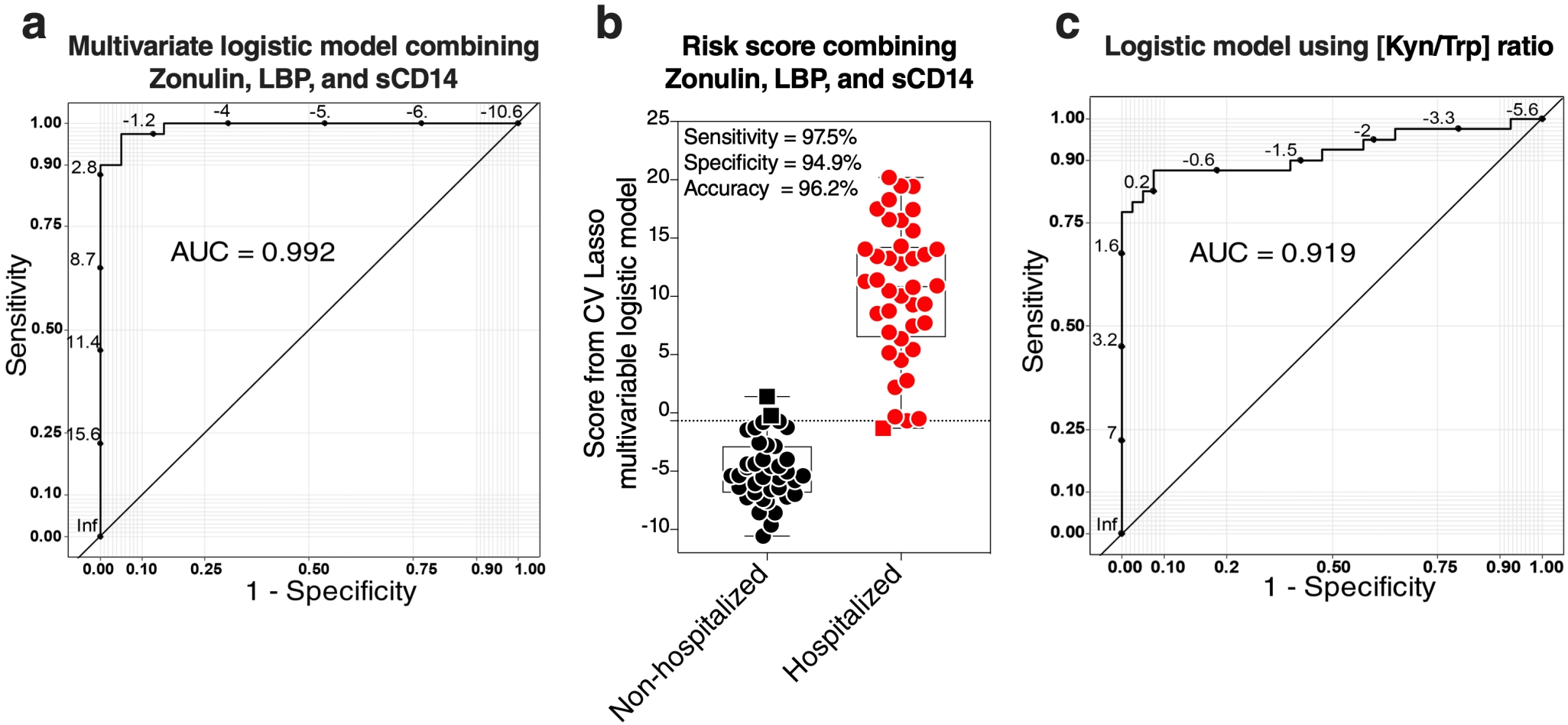
a
Multivariate logistic model combining Zonulin, LBP, and sCD14
AUC = 0.992
Sensitivity
1 - Specificity
b
Risk score combining Zonulin, LBP, and sCD14
Sensitivity = 97.5%
Specificity = 94.9%
Accuracy = 96.2%
Score from CV Lasso multivariable logistic model
Non-hospitalized
Hospitalized
c
Logistic model using [Kyn/Trp] ratio
AUC = 0.919
Sensitivity
1 - Specificity

Table 1. Levels of the 35 out of 50 gut- and gut microbiota-associated plasma metabolites that are disrupted during COVID-19

	log_2 ratio						FDR					
Group	Mild	Moderate	Severe	Moderate	Severe	Severe	Mild	Moderate	Severe	Moderate	Severe	Severe
Compared to group	Control	Control	Control	Mild	Mild	Moderate	Control	Control	Control	Mild	Mild	Moderate
2,3-Dihydroxybenzoic acid	-0.09	-1.78	0.02	-1.70	0.11	1.81	0.64	0.0002	0.003	0.015	0.033	0.76
Decanoic acid	-0.04	-1.68	-1.32	-1.64	-1.28	0.36	0.90	0.004	0.009	0.0006	0.001	0.98
(2R)-2,3-Dihydroxypropanoic acid	-0.57	-1.39	-2.30	-0.81	-1.73	-0.91	0.39	0.0005	$8x10^{-6}$	0.004	$3x10^{-5}$	0.78
Indole-3-acetic acid	-0.50	-1.31	-0.86	-0.81	-0.36	0.45	0.39	0.0002	0.001	0.007	0.023	0.92
Pipecolic acid	-0.34	-1.02	-1.56	-0.68	-1.21	-0.53	0.55	0.008	0.0002	0.24	0.012	0.48
Hippuric acid	-0.49	-1.02	0.59	-0.54	1.07	1.61	0.98	0.021	0.10	0.028	0.14	0.94
2,4-Dihydroxybenzoic acid	-0.67	-0.99	-2.67	-0.32	-1.99	-1.67	0.39	0.002	$4x10^{-6}$	0.039	$7x10^{-5}$	0.85
Indole-3-pyruvic acid	-0.09	-0.90	-1.35	-0.81	-1.26	-0.46	0.98	0.001	$1x10^{-5}$	0.004	$9x10^{-5}$	0.68
3-methylphenylacetic acid	-0.52	-0.75	-0.77	-0.23	-0.25	-0.02	0.64	0.031	0.013	0.56	0.84	0.92
L-Tryptophan	-0.04	-0.65	-0.91	-0.62	-0.88	-0.26	0.93	0.0001	$2x10^{-6}$	0.0006	$4x10^{-6}$	0.68
Citrulline	0.04	-0.57	-1.08	-0.61	-1.12	-0.51	0.95	0.002	$5x10^{-6}$	0.003	$6x10^{-6}$	0.51
Deoxycholic Acid	-0.68	-0.45	-1.42	0.23	-0.74	-0.97	0.98	0.29	0.020	0.19	0.016	0.71
Pyruvic acid	0.03	-0.37	-0.52	-0.40	-0.54	-0.15	0.96	0.020	0.001	0.013	0.0006	0.76
L-Serine	-0.36	-0.30	-0.61	0.06	-0.25	-0.31	0.39	0.079	0.001	0.78	0.18	0.51
4-Hydroxybenzaldehyde	0.00	-0.28	-0.31	-0.28	-0.31	-0.03	0.90	0.009	0.018	0.21	0.16	0.95
L-Threonine	-0.05	-0.22	-0.39	-0.17	-0.34	-0.17	0.88	0.035	0.002	0.047	0.002	0.76
2-Hydroxycinnamic acid	-0.02	-0.19	-0.27	-0.17	-0.25	-0.08	0.87	0.016	0.012	0.27	0.16	0.98
Glycine	-0.12	0.02	-0.58	0.14	-0.46	-0.60	0.78	0.062	0.001	0.41	0.027	0.51
Allantoin	-0.09	0.14	-0.55	0.23	-0.45	-0.69	0.96	0.25	0.010	0.27	0.017	0.53
4-Hydroxyproline	-0.04	0.29	0.11	0.33	0.15	-0.18	0.90	0.020	0.67	0.018	0.93	0.48
Glycyl-L-leucine	-0.08	0.34	0.68	0.42	0.76	0.34	0.93	0.49	0.056	0.31	0.036	0.68
Choline	-0.23	0.35	0.63	0.58	0.86	0.28	0.39	0.32	0.010	0.025	0.0003	0.68
2-Hydroxyhippuric acid	-0.98	0.64	2.42	1.61	3.40	1.79	0.49	0.075	0.028	0.73	0.24	0.76
trans-Cinnamic acid	-0.13	0.66	0.39	0.80	0.53	-0.27	0.59	0.022	0.012	0.004	0.003	0.95
Succinic acid	-0.02	0.68	1.49	0.70	1.51	0.81	0.64	0.023	$7x10^{-5}$	0.037	$2x10^{-5}$	0.48
Phosphoenolpyruvic acid	-0.11	0.70	1.01	0.82	1.12	0.30	0.74	0.013	0.0003	0.010	$7x10^{-5}$	0.68
Acetylcholine	-0.02	0.72	0.55	0.74	0.57	-0.17	0.69	0.028	0.053	0.012	0.036	0.92
L-Lactic acid	-0.06	0.91	1.29	0.96	1.35	0.39	0.90	0.0002	$2x10^{-5}$	0.0001	$7x10^{-5}$	0.48
L-Kynurenine	0.28	0.96	1.20	0.69	0.93	0.24	0.39	0.002	$5x10^{-5}$	0.024	0.002	0.68
16-Hydroxyhexadecanoic acid	0.94	1.46	1.19	0.52	0.25	-0.27	0.39	0.0002	0.0008	0.16	0.24	0.90
2-Hydroxyvaleric acid	1.12	1.57	1.63	0.45	0.51	0.07	0.79	0.003	0.0004	0.025	0.016	0.94
Glucose 6-phosphate	0.04	1.93	2.55	1.89	2.51	0.62	0.64	$2x10^{-5}$	$3x10^{-6}$	$1x10^{-5}$	$4x10^{-6}$	0.48
Kynurenic acid	0.00	2.29	2.53	2.29	2.54	0.24	0.79	0.60	0.008	0.69	0.034	0.68
ß-D-Glucopyranuronic acid	0.01	2.64	2.77	2.63	2.76	0.13	0.69	0.088	0.0002	0.27	$9x10^{-5}$	0.68
3-Hydroxybutyric acid	0.91	2.88	3.66	1.97	2.75	0.78	0.90	0.002	$5x10^{-6}$	0.010	$7x10^{-5}$	0.70

Table 2. Logistic regression models of tight junction permeability and microbial translocation markers for their ability to distinguish hospitalized from non-hospitalized individuals.

Variables	AUC	SE	95% Confidence interval		P-value (single predictor models vs. Lasso selected multivariable model)
Variables identified by Lasso multivariable logistic model	0.992	0	0.981	1.000	reference
Zonulin	0.951	0	0.901	1.000	0.0656
LBP	0.944	0	0.885	1.000	0.0987
βglucan	0.841	0	0.748	0.933	0.0008
sCD14	0.930	0	0.871	0.988	0.0323
Occludin	0.663	0.1	0.542	0.783	<0.0001
Reg3A	0.635	0.1	0.510	0.759	<0.0001
sCD163	0.627	0.1	0.503	0.751	<0.0001
IFABP	0.538	0.1	0.408	0.668	<0.0001

Bold variables are variables selected by Lasso to be included in the multivariable logistic model; AUC = Area under the ROC Curve; SE = Standard error